

Quantum chemistry-based interpretations on the lowest triplet state of luminescent lanthanides complexes. Part 1. Relation between the triplet state energy of hydroxamate complexes and their luminescence properties

Fabien Gutierrez,^a Christine Tedeschi,^b Laurent Maron,^a Jean-Pierre Daudey,^a Romuald Poteau,^{*a} Joëlle Azema,^b Pierre Tisnès^b and Claude Picard^{*b}

^a Laboratoire de Physique Quantique (UMR5626 du CNRS), IRSAMC.

E-mail: romuald.poteau@irsamc.ups-tlse.fr

^b Laboratoire de Synthèse et Physico-Chimie de Molécules d'Intérêt Biologique (UMR5068 du CNRS) Université Paul Sabatier, 118 route de Narbonne, 31062 Toulouse Cedex, France. E-mail: picard@chimie.ups-tlse.fr

Received 12th December 2003, Accepted 17th February 2004

First published as an Advance Article on the web 23rd March 2004

In this paper, we evaluate the potential use of theoretical calculations to obtain an energy scale of the lowest ligand-centred triplet excited state in luminescent terbium(III) complexes. In these complexes, non-radiative deactivation of the terbium emitting state *via* a back-energy transfer process ($T_1 \leftarrow \text{Tb}({}^5\text{D}_4)$) is a common quenching process. Consequently the prediction of the energy gap between these two excited states should be useful for programming highly luminescent Tb^{III} systems. We report on a strategy based upon experimental and theoretical investigations of the excited state properties of a series of four simple aromatic hydroxamate ligands coordinated to Tb^{III} and Gd^{III} ions. By using previously reported crystallographic data, the structural and energies properties of these systems were investigated in the ground and first excited triplet states at the density functional theory (DFT) level of calculations. Our theoretical results are consistent with a triplet excited state T_1 which is localised on one ligand only and whose the energy level is independent of the lanthanide ion nature (Tb^{III}, Gd^{III}). A good agreement between the calculated adiabatic transition energies and experimental data derived from emission spectra is obtained when a corrective term is considered. These satisfactory results are an indication that this type of modelling can lead to discriminate in terms of the position of the lowest ligand triplet energy level the best antenna among a family of chromophoric compounds. In addition this theoretical approach has provided indications that the difference between the adiabatic transition energies of all the investigated complexes can be mainly explained by metal–ligand electrostatic interactions. The influence of the number of antennae on the quantum yield and the luminescence lifetime is discussed.

1 Introduction

Trivalent lanthanide ions Ln^{III} are able to form stable complexes with a wide variety of organic ligands. These complexes, which show interesting magnetic and spectroscopic properties, are used in many fields. In so far as we are dealing in this paper with the luminescent properties of lanthanide complexes, it must be underlined that their long-lived luminescence lifetimes and the “renaissance of fluorescence energy transfer”¹ have played a significant role in the interest devoted to these systems. Although most of the systems designed for biomedical tests essentially involve terbium and europium complexes, recent developments of multiple fluoroimmunoassays require to consider other lanthanide ions, such as samarium or ytterbium.^{2,3}

Lanthanide complexes are considered as light converter molecular devices (LCMDs), since they are able to absorb UV light and to emit a radiation in the near-IR or visible domain. However, although the involved emitting states are the electronic levels of the lanthanide ion, free lanthanide ions in solution do not behave as efficient LCMDs. As a matter of fact, the absorption of lanthanide ions in water is very inefficient, the molar absorption coefficient being measured with an order of magnitude less than 10 dm³ mol⁻¹ cm⁻¹. Thus, the excited states of the ion must be more efficiently populated. This is achieved by complexing the Ln^{III} ion by ligands which act as photosensitizers. It was initially reported by Weissman in 1942⁴ and has been more recently referred to an antenna effect.⁵ While the basic mechanism for luminescence has often been reviewed,^{5,6} a brief recalling is necessary for understanding the purpose of this work.

The lowest excited states of the lanthanide ions involve the reorganisation of the electrons within the 4f shell. It is now well known that the 4f electrons can be considered as core electrons when dealing with chemical bonding.⁷ The role of the ligands is on one hand to collect the photons provided by the light source in order to allow an energy transfer to the emitting levels of the Ln^{III} ion, and on the other to shield it against the solvent in order to avoid non-radiative deactivation processes. In addition, synergistic ligands can be used in order to completely remove water from the first solvation shell of the lanthanide ion.^{8,9} The intramolecular photochemical pathways which can be followed are summarized in Fig. 1 in the form of a Jablonski

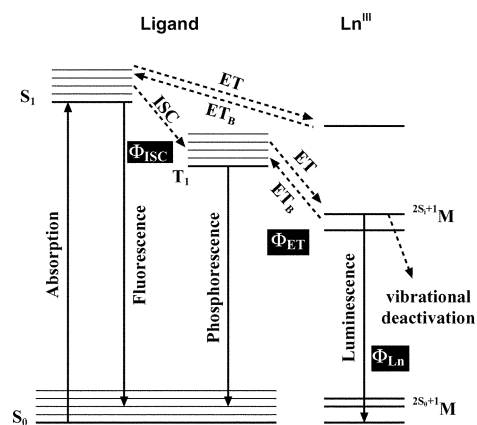


Fig. 1 Photochemical pathways.

diagram. The most probable channel corresponds to (i) the absorption of UV light by the organic chromophore, (ii) an intersystem crossing (ISC) from the excited singlet state to a triplet state of the ligand, (iii) an intramolecular energy transfer from the triplet state to the closest emitting level of the metal, (iv) a radiative transition in the visible or near-IR domains, which is called luminescence in order to be distinguished from the emission of light of organic fluorophores. It should be emphasized that transitions between the f states are formally parity forbidden (Laporte rule), which results in the long radiative lifetimes (up to the millisecond timescale) and line-like emission bands which all together make the interest of lanthanide complexes. Steps (ii), (iii) and (iv) are characterized by Φ_{ISC} , Φ_{ET} and Φ_{Ln} quantum yields, respectively (see Fig. 1), the total quantum yield being defined as $\Phi = \Phi_{\text{ISC}}\Phi_{\text{ET}}\Phi_{\text{Ln}}$.

At this point, some important remarks should be stressed. From an experimental point of view, it is not clear whether the energy transfer occurs from an excited singlet or triplet state. However, Malta and co-workers have shown with a kinetic model that in several cases the energy transfer channel singlet (ligand) \rightarrow emitting level of Ln^{III} is not important.^{10,11} The triplet state thus plays a leading role in the intensity of the luminescence, indirectly confirmed by experimental evidences. An empirical rule, hereafter called the energy-gap rule, states that the total luminescence quantum yield Φ decreases due to an energy back-transfer (ET_B, see Fig. 1) when the energy difference between the lowest triplet state of the ligand and the emitting level of the metal is small. This is in particular supported by the extensive study of Latva *et al.*¹² which has clearly shown in the case of terbium complexes a correlation between the lowest triplet state energy level of the ligand (T₁) and Tb^{III} luminescence quantum yield. The empirical rule states that a high luminescence quantum yield is unlikely to be observed if the energy gap between the T₁ level of the ligand and the excited ⁵D₄ level of terbium is less than about 1850 cm⁻¹. It should be noticed that in the case of europium complexes, the correlation between the energy levels of the T₁ state and the luminescence quantum yield is less convincing. As a matter of fact, the presence of other ⁵D_j resonance levels higher than the emitting ⁵D₀ level is probably responsible for the dispersion of the results. More recently, Arnaud and Georges¹³ have compared the luminescent properties of europium and terbium complexes with the values reported by Latva *et al.* They have shown again that the luminescence lifetimes are closely related to the energy gap between the ligand triplet and the resonance energy levels of the metal ion. Archer *et al.*¹⁴ also found results consistent with the triplet state channel since they obtained very low quantum yields for europium complexes with a T₁ level below the ⁵D₀ level.

Although we have underlined the important role of the lowest triplet state of the complexed ligand, other factors can strongly influence the Ln^{III} luminescence and even overcome the triplet state factor. Quenching mechanisms induced by the presence of solvent molecules in the first solvation sphere or by ligand-to-metal charge transfer (LMCT) states are also known to be of great importance.⁵ In this latter case, which is very likely to occur for europium complexes, the triplet state is very little populated since there is a competition with the LMCT states.^{15,16}

The interest generated by the wide range of applications of luminescent lanthanide complexes explains that the design of efficient molecular edifices is still an important research goal. However, the photophysical processes involved in their optical activity are rather complex and intrinsically tangled, and chemical intuition may not be sufficient to design efficient luminescent complexes. There is probably a need for giving a theoretical point of view in order to understand the mechanisms involved, and to provide a “*in silico*” screening of lanthanide compounds. To our knowledge, there is very little theoretical work about the spectroscopic properties of such

complexes. On one hand, the Malta group has provided theoretical insights, by combining various approaches: ligand field theory for evaluating the 4f–4f intensities, semi-empirical methods for the calculation of the ligand excited states, and a kinetic model for the determination of intramolecular energy transfer rates. On the other hand, very comprehensive studies have been reported for excited state levels of An and Ln complexes, but only in the case of metal-to-metal transitions.¹⁷ To our knowledge, this contribution is the first trying to reproduce, for Ln complexes, the excited electronic spectra involving LMCT phenomena.

We have considered, experimentally and theoretically, the excited state properties of hydroxamate ligands coordinated to Tb^{III} and Gd^{III} ions. Such [CO–N(R)O]⁻ anionic ligands (L⁻) behave as bidentate {O,O} ligands. 1-Hydroxypyridin-2-one (Fig. 2(a)) forms 3 : 1 complexes with lanthanide ions which have been structurally characterized by X-ray experiments.^{18,19} Moreover, this ligand acts as a better sensitizer for Tb^{III} with respect to Eu^{III}. Since such hydroxamate ligands show interesting potential as new types of building blocks for LCMD devices, we report in this paper new experimental results concerning three other ligands (Fig. 2(b)–(d)), combined with theoretical investigations of the structural and energetic properties of these systems in their ground and first excited triplet states, S₀ and T₁. In the present theoretical contribution, we have applied *ab initio* and DFT calculations in order to obtain an energy scale of the lowest triplet state of the ligands, and also to understand the nature of the lowest triplet state.

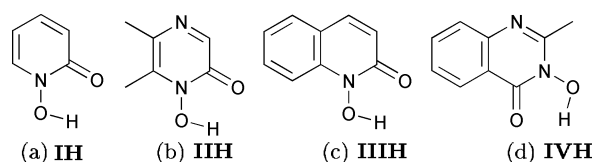


Fig. 2 Hydroxamic acids (LH). The hydroxyl group is deprotonated in hydroxamate ligands (L⁻): (a) 1-hydroxypyridin-2-one, (b) 1-hydroxy-5,6-dimethylpyrazin-2-one, (c) 1-hydroxyquinolin-2-one, (d) 3-hydroxy-2-methylquinazolin-4-one.

2 Experimental and computational details

2.1 Experimental

Materials and synthesis. Lanthanide salts were purchased from Aldrich (GdCl₃·6H₂O, TbCl₃·6H₂O) or Strem Chemicals (Tb₂(CO₃)₃·xH₂O) and were used without further purification.

1-Hydroxypyridin-2-one, **IH.** This was purchased from Aldrich and was purified as previously described.¹⁹ Mp 148–149 °C (lit.,²⁰ 149–150 °C). Found: C, 54.10; H, 4.40; N, 12.52. C₅H₅NO₂ requires C, 54.06; H, 4.54; N, 12.61%. IR ν /dm⁻¹: 1637 (C=O), UV (CH₃OH) λ /nm (ϵ /dm³ mol⁻¹ cm⁻¹): 203, 232 (6500), 310 (4500).

1-Hydroxy-5,6-dimethylpyrazin-2-one, **IIH.** This compound was prepared in four steps by using procedures described in the literature.²¹ *N*-(*tert*-Butoxycarbonyl)glycine was coupled with *O*-benzylhydroxylamine by using the mixed carbonic anhydride method with isobutylchloroformate. Deprotection of the Boc group by trifluoroacetic acid in dichloromethane, followed by condensation of the resulting salt with 2,3-butanedione gave compound **IIH**, O-protected by a benzyl group. Debenzylation by catalytic hydrogenation on 5% Pd/C and subsequent purification on a silica gel column using CHCl₃–MeOH–NH₄OH (6 : 3 : 1) as eluent afforded the pure product **IIH**. Mp 150–152 °C (lit.,²¹ 147–149 °C). Found: C, 51.25; H, 5.68; N, 19.76. C₆H₈N₂O₂ requires C, 51.42; H, 5.75; N, 19.99%. IR ν /cm⁻¹: 3270 (OH), 1729 (C=O), 1578 (C=N). ¹H NMR (CD₃OD) δ /ppm: 2.36 (s, 3H), 2.43 (s, 3H), 7.71 (s, 1H). UV (CH₃OH) λ /nm (ϵ /dm³ mol⁻¹ cm⁻¹): 232 (16300), 339 (5300).

1-Hydroxyquinolin-2-one, **IIIH.** A procedure similar to that reported by Raban *et al.*²² was used. To a solution of quinoline

N-oxide (1.011 g, 6.97 mmol) in benzene (60 mL) was added calcium carbonate (0.6 g, 6 mmol) and lead tetraacetate (5 g, 11.28 mmol). The mixture was heated at reflux for 3 h. The reaction was allowed to cool to room temperature and the solid was collected and washed with chloroform (50 mL). The combined filtrates were concentrated under reduced pressure. The residue was dissolved in 10% hydrochloric acid (30 mL). The aqueous solution was heated at reflux for 1 h, cooled and extracted with diethyl ether (2 × 50 mL). The organic phase was concentrated *in vacuo* and the solid residue was sublimed (100 °C/26 mbar). Yield 35%. Mp 190–191 °C (lit.,²² 186–189 °C). Found: C, 66.53; H, 4.32; N, 8.59. C₉H₇NO₂ requires C, 67.08; H, 4.38; N, 8.69%. IR ν/cm^{-1} : 2504 (OH), 1636 (C=O), 1581 and 1558 (C=C and C=N). ¹H NMR (CD₃OD): δ/ppm 6.74 (d, $J = 9.5$ Hz, 1H), 7.28–7.36 (m, 1H), 7.71–7.82 (m, 3H), 7.94 (d, $J = 9.5$ Hz, 1H). UV (CH₃OH) λ/nm ($\epsilon/\text{dm}^3 \text{ mol}^{-1} \text{ cm}^{-1}$): 231 (38400), 271 (5200), 331 (5000).

3-Hydroxy-2-methylquinazolin-4-one, IVH. This compound was prepared in three steps starting from isatoic anhydride. The reaction of *O*-benzylhydroxylamine with isatoic anhydride in aqueous solution gave the corresponding hydroxamate (2-amino-*N*-benzyloxybenzamide). Cyclisation with acetic anhydride gave compound **IVH**, O-protected by a benzyl group. Debenzoylation was then performed by catalytic hydrogenation.

2-Amino-*N*-benzyloxybenzamide. To a solution of *O*-benzylhydroxylamine hydrochloride (2.160 g, 12.58 mmol) in water (60 mL) was slowly added 0.935 g of K₂CO₃. This mixture was stirred for 0.5 h and then was added isatoic anhydride (2 g, 12.3 mmol). The reaction mixture was kept at room temperature under stirring for 24 h and was then filtered. The solid was dried under vacuum and then recrystallized from CH₂Cl₂. Yield 95%. Mp 104–105 °C (lit.,²³ 104–106 °C). Found: C, 68.84; H, 5.71; N, 11.41. C₁₄H₁₄N₂O₂ requires C, 69.41; H, 5.82; N, 11.56%. ¹H NMR (CDCl₃) δ/ppm : 5.00 (s, 2H), 5.36 (s, 2H), 6.57 (t, $J = 7.5$ Hz, 1H), 6.66 (d, $J = 7.5$ Hz, 1H), 7.13–7.26 (m, 2H), 7.36–7.47 (m, 5H), 8.55 (s, 1H). ¹³C NMR (CDCl₃) δ/ppm : 78.4, 113.0, 116.6, 117.3, 127.1, 128.3, 128.4, 128.7, 133.0, 135.5, 148.8, 168.4.

3-Benzyloxy-2-methylquinazolin-4-one. A mixture of 2-amino-*N*-benzyloxybenzamide (2 g, 8.25 mmol) and acetic anhydride (9.12 mL, 8.3 mmol) was heated under reflux for 2 h. After cooling, water (3.9 mL) and activated carbon were added and the mixture was boiled for a further 0.5 h, followed by filtration through a Celite pad. The Celite pad was washed with methanol and the combined filtrates were evaporated under reduced pressure. The residue was subjected to column chromatography on silica gel (CH₂Cl₂–MeOH, 90 : 10) to give the desired product. Yield 39%. Mp 111–112 °C (lit.,²³ 110–112 °C). Found: C, 71.93; H, 5.35; N, 10.36. C₁₆H₁₄N₂O₂ requires C, 72.17; H, 5.30; N, 10.52%. ¹H NMR (CDCl₃) δ/ppm : 2.48 (s, 3H), 5.29 (s, 2H), 7.40–7.53 (m, 6H), 7.63 (d, $J = 7.5$ Hz, 1H), 7.74 (td, $J = 7.5, 1.5$ Hz, 1H), 8.30 (dd, $J = 7.5, 1.5$ Hz, 1H). ¹³C NMR (CDCl₃) δ/ppm : 20.4, 78.3, 122.6, 126.5, 126.7, 127.1, 128.9, 129.6, 130.0, 133.4, 134.4, 146.5, 153.9, 158.2.

Compound IVH. 10% Pd/C (60 mg) suspended in MeOH (10 mL) was prehydrogenated with H₂ for 0.5 h. To the suspension was then added a solution of previous *O*-benzyl protected compound (0.429 g, 1.61 mmol) in MeOH (15 mL). After hydrogenation at room temperature with H₂ under atmospheric pressure for 0.25 h, the mixture was filtered through a Celite pad. The filtrate was evaporated to give a solid residue which was purified by recrystallisation from a MeOH–water mixture. Yield 16%. Mp 218–219 °C. Found: C, 60.88; H, 4.49; N, 15.78. C₉H₈N₂O₂ requires C, 61.36; H, 4.58; N, 15.90%. IR ν/cm^{-1} : 2561 (OH), 1684 (C=O), 1610 and 1564 (C=C and C=N). ¹H NMR (DMSO) δ/ppm : 2.51 (s, 3H), 7.49 (t, $J = 7.7$ Hz, 1H), 7.61 (d, $J = 8.1$ Hz, 1H), 7.79 (t, $J = 8.1$ Hz, 1H), 8.11 (d, $J = 7.7$ Hz, 1H). ¹³C NMR (DMSO) δ/ppm : 20.2, 121.3, 125.7, 125.9, 126.6, 133.8, 146.1, 154.2, 157.7. UV (CH₃OH) λ/nm ($\epsilon/\text{dm}^3 \text{ mol}^{-1} \text{ cm}^{-1}$): 221, 314 (24100).

Terbium complexes. The TbI₃·3H₂O complex was isolated as previously described.¹⁹ Found: C, 33.26; H, 3.03; N, 7.66. C₁₅H₁₈N₃O₉Tb requires C, 33.16; H, 3.34; N, 7.73%. IR ν/cm^{-1} : 1621 (C=O).

The TbIII₃·2H₂O complex was isolated according to the following procedure: to a solution of Tb₂(CO₃)₃·xH₂O (25.6 mg) in ethanol (1 mL) was added ligand **III** (50 mg, 0.31 mmol). The mixture was stirred for 2 h and filtered. The solid residue was washed with three portions of ethanol (3 × 2 mL), and then several times with methanol. The combined methanol extracts were evaporated. The desired product was purified by recrystallisation from water. Found: C, 47.98; H, 3.38; N, 6.22. C₂₇H₂₂N₃O₈Tb requires C, 48.02; H, 3.28; N, 6.22%. IR ν/cm^{-1} : 1613 (C=O).

Preparation 'in situ' of the terbium complexes. To a solution of a sample of each bidentate ligands **IIH–IVH** in methanol was added an equimolar amount of NaOH. Subsequently, a solution of TbCl₃·6H₂O (0.33 equivalent) in methanol was added and the reaction mixture was allowed to stir for 3 h at room temperature. The concentrations used for photophysical measurements were between 5×10^{-6} and $1 \times 10^{-4} \text{ mol dm}^{-3}$.

TbI₃: UV (CH₃OH) λ/nm ($\epsilon/\text{dm}^3 \text{ mol}^{-1} \text{ cm}^{-1}$): 221, 310 (12000). Luminescence (CH₃OH, 295 K, $\lambda_{\text{exc}} = 310 \text{ nm}$): λ/nm 491 (relative intensity, 26.5), 548 (100), 588 (14.9), 622 (7.6).

TbII₃: UV (CH₃OH) λ/nm ($\epsilon/\text{dm}^3 \text{ mol}^{-1} \text{ cm}^{-1}$): 227, 333 (12600). Luminescence (CH₃OH, 295 K, $\lambda_{\text{exc}} = 330 \text{ nm}$): λ/nm 490 (relative intensity, 30.2), 547 (100), 588 (17.5), 622 (10.4).

TbIII₃: UV (CH₃OH) λ/nm ($\epsilon/\text{dm}^3 \text{ mol}^{-1} \text{ cm}^{-1}$): 245 (107100), 347 (10800). Luminescence (CH₃OH, 295 K, $\lambda_{\text{exc}} = 345 \text{ nm}$): λ/nm 491 (relative intensity, 40.6), 547 (100), 588 (25.4), 619 (23.8).

TbIV₃: UV (CH₃OH) λ/nm ($\epsilon/\text{dm}^3 \text{ mol}^{-1} \text{ cm}^{-1}$): 220, 255 (70200), 310 (16200). Luminescence (CH₃OH, 295 K, $\lambda_{\text{exc}} = 310 \text{ nm}$): λ/nm 489 (relative intensity, 32.0), 546 (100), 586 (22.3), 620 (21.5).

The gadolinium complexes were prepared 'in situ' according to the procedure described for terbium complexes.

Instruments and measurements. Melting points were determined on a Kofler apparatus. ¹H and ¹³C magnetic resonance spectra were recorded on a Bruker 250 spectrometer. IR spectra were recorded on a Perkin-Elmer spectrometer in potassium bromide pellets. Elemental analyses were carried out by the "Service Commun de Microanalyse élémentaire UPS-INP" in Toulouse.

Electronic spectra in the UV-visible range were recorded at 295 K with a Perkin-Elmer Lambda 17 spectrophotometer using quartz cells of various path lengths. Time-resolved luminescence spectra and life-times were obtained using a LS-50B Perkin-Elmer spectrofluorimeter equipped with a Hamamatsu R928 photomultiplier tube and the low-temperature accessory No L2250136. For excitation a xenon flash lamp, pulsed at line frequency (60 Hz) was used. The most highly resolved emission spectra were obtained using excitation and emission slit widths of 2.5 nm, following pulsed excitation at the lowest energy ligand-centered absorption band. Emission spectra were corrected from the wavelength dependence of the photomultiplier tube, according to the instrument guidebook. Lifetimes τ (uncertainty $\leq 5\%$) are the average values from at least five separate measurements which were made by monitoring the decay at 545 nm, following pulsed excitation. The emission decay curves were fitted by an equation of the form $I(t) = I(0)\exp(-t/\tau)$ using a curve-fitting program. Luminescence quantum yields (uncertainty $\pm 15\%$) were determined by the method described by Haas and Stein,²⁴ using as standard quinine sulfate in 1 N sulfuric acid ($\Phi = 0.546^{25}$) and corrected for the refractive index of the solvent. The absorbance of the solutions was 0.1 at the excitation wavelength. The lifetimes and luminescence spectra were recorded in aerated methanol previously dried over molecular sieves (3 Å) and by using freshly

prepared samples. The phosphorescence spectra of the ligands and of their Gd(III) complexes were recorded in an ethanol–methanol mixture (4 : 1) at 77 K (liquid N₂ cooling).

2.2 Computational

All calculations of the molecules in their ground state (S_0) and their three lowest excited triplet states (T_i , $i = 1, 2, 3$) were carried out with Gaussian 98.²⁶ As usually done in quantum chemistry calculations, the methyl groups of ligands **II** and **IV** were replaced by hydrogen atoms. These ligands will be hereafter denoted **II'** and **IV'**. All calculations were done in the gas phase. The effective core potentials (ECPs) and their associated basis set developed by the Stuttgart group were used in the case of terbium, gadolinium and sodium atoms.^{27,28} In LnL₃ compounds, the electronic configuration of the lanthanide(III) ion is [Kr]4f¹⁰5s²5p⁶4f^{*n*-1}, and it is now well known that 4f and 4d electrons do not play any role in the coordination of the ion.^{7,29} The goal of this work is not to calculate the electronic states of the metal ion (M), but to get the lowest excited states of the complex. These states can either be strictly localized on the ligands (L) or can be ligand-to-metal charge transfer type ones (LMCT states), involving back-donation towards 5d atomic orbitals. As a consequence, we used large core ECPs with 11 valence electrons, specifically designed for rare earth atoms with an oxidation number +3 (Ln^{III}). All the gaussian basis sets are of double- ζ plus polarization quality. All structures were optimized in their lowest triplet state (T_1) and their ground state (S_0) without symmetry constraints, in order to avoid explorations of potential energy surfaces driven by such constraints. We systematically explored the potential energy surfaces in the framework of density functional theory (DFT) methods, using the B3LYP functional. The lowest triplet state has essentially been investigated with unrestricted DFT methods. Calculating energy gaps between the optimized unrestricted DFT triplet and restricted DFT singlet geometries is the so-called Δ SCF procedure. However, preliminary geometry optimizations of some molecules in T_1 were also performed by means of the *ab initio* CASSCF method,³⁰ in order to check the validity of single-configuration approaches. Spin contamination is not so severe with unrestricted DFT calculations as in unrestricted Hartree–Fock methods, the eigenvalue of \hat{S}^2 for T_1 lying between 2.00 and 2.06. However, Kohn–Sham molecular orbitals (MOs) obtained at an unrestricted DFT level of calculation do not allow a clear analysis of the nature of the triplet state. Time-dependent DFT (TDDFT) calculations were also performed to provide an overview of the nature of the T_1 state. TDDFT is currently undergoing a growing interest. Even if according to some authors this method experiences some difficulties for the description of Rydberg and charge transfer states,³¹ it appears very successful for evaluating vertical electronic transitions,^{32–34} and even charge transfer states in metal complexes.³⁵

Finding the optimal geometry of lanthanide complexes is not a trivial task. However, it will be shown hereafter in section 3 that the four terbium–hydroxamate complexes are very likely isostructural. We consequently have used the crystallographic data previously published for terbium¹⁸ and gadolinium¹⁹ complexes with 1-oxy-2-pyridinonate (ligand **I'**) as a starting point for geometry optimizations. These data, together with the Z-matrix editor functionality of the MOLDEN program,³⁶ were also helpful for constructing the geometries of the three other ligands. For the purpose of comparison with phosphorescence spectra, we have also checked in some cases that relaxing in S_0 the optimal structure of the molecule found for T_1 leads to the optimal geometry deduced from the terbium and gadolinium X-ray structures. In other words, in the case of such simple ligands, when the molecule goes back from T_1 to the ground state it is not trapped into a local minimum that differs from the optimal geometry in S_0 . Due to the size of the largest

Table 1 Absorption and luminescence properties of the Tb^{III} complexes derived from ligands **I–IV** in aerated methanol solution at 295 K; τ_H and τ_D are the luminescent lifetimes in CH₃OH and CH₃OD, respectively

L	λ_{\max}/nm	$\epsilon/\text{dm}^3 \text{ mol}^{-1} \text{ cm}^{-1}$	τ_H/ms	τ_D/ms	Φ
I	312	12000	0.83	1.06	0.20
II	333	12600	0.92	1.16	0.001
III	347	10800	0.93	1.25	0.001
IV	310	16200	0.80	0.96	0.023

complexes, calculation of zero-point-energies were not systematically feasible and experimental $\tilde{\nu}_{00}$ wavenumbers will be compared to theoretical adiabatic wavenumbers $\tilde{\nu}_{\text{adia}}$ unless otherwise mentioned (Fig. 3).

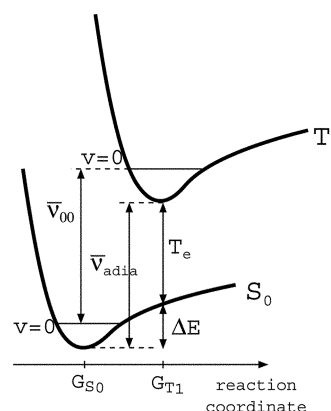


Fig. 3 Schematic definition of the computed transitions and the corresponding wavelengths; $\tilde{\nu}_{\text{adia}}$ is calculated as $E(T_1, G_{T_1}) - E(S_0, G_{S_0})$, whereas ΔE and T_e are calculated as $E(S_0, G_{T_1}) - E(S_0, G_{S_0})$ and $E(T_1, G_{T_1}) - E(S_0, G_{T_1})$, respectively (in the framework of the same theoretical method, $\tilde{\nu}_{\text{adia}}$ and $T_e + \Delta E$ are equal).

The molecules and molecular orbitals sketches were drawn with the MOLEKEL program.³⁷ Finally, in so far as the R groups defining the four [CO–N(R)OH] acids considered in this work are different, a comparison between their structures do not provide relevant information, and we shall only comment the geometrical parameters and electronic charges of the four atoms which form a ring with the metal ion in the complexes (Fig. 4).

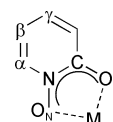


Fig. 4 Definition of the labels of the atoms.

3 Experimental results

We first isolated the complexes Tb**I**₃ and Tb**III**₃ (See Experimental section) but soon noticed that their emitting properties in solution are identical with those of mixtures of the ligands and TbCl₃·6H₂O in the presence of sodium hydroxide (3 : 1 : 3 equivalents, respectively). The mixtures give absorption and excitation spectra identical with those of the isolated complexes, we thus employed the latter method for this photophysical study. All the photophysical data collected in Table 1 were obtained by using methanol solutions. The absorption spectra of these complexes are characterized by intense bands in the UV region. Deprotonation of the ligand and its subsequent bridging to the metal ion has a marked effect on the absorption profile. For example, free ligand **IIIH** in methanol solution exhibits three distinct absorption bands with maxima around 231, 271 and 331 nm, while the spectrum of the corresponding complex is composed of two absorption bands at 245

and 347 nm. On the other hand, it can be noticed that the molar absorption coefficient at the maximum of the ligand-centered (LC) band ($310 \text{ nm} < \lambda < 347 \text{ nm}$) is higher than $10^4 \text{ dm}^3 \text{ mol}^{-1} \text{ cm}^{-1}$ for all these complexes, a favourable condition for an efficient antenna effect. The Beer-Lambert law is obeyed in the used range of concentrations (5×10^{-6} to $1 \times 10^{-4} \text{ mol dm}^{-3}$) which confirms the stability of the complexed species in methanol. Photoexcitation of the complexes from the lowest energy LC absorption band gives rise to the typical Tb^{III} luminescence with an intense emission band around 545 nm, and three weaker bands around 490, 590 and 620 nm. These bands correspond to the transitions from the $^5\text{D}_4$ state to the $^7\text{F}_6$, $^7\text{F}_5$, $^7\text{F}_4$ and $^7\text{F}_3$ levels, respectively. The emission spectra and relative peak heights of terbium emission with all chelates are essentially identical, in agreement with the fact that the terbium emission bands are not very sensitive to changes outside the first coordination sphere.³⁸ On the other hand, although these complexes have similar molar extinction coefficients at λ_{max} , the total luminescence intensity is chelate dependent. Excitation spectra of Tb^{III} emission are dominated by broad bands corresponding to the absorptions of the aromatic hydroxamate moieties. No transition corresponding to the proper Tb^{III} absorption levels, especially those located at 485 nm and between 340 and 380 nm, is observable in the excitation spectra. These results unequivocally show that an energy transfer process from the hydroxamate antenna to the metal ion is the only photophysical pathway leading to observable luminescence in these samples. Representative excitation and emission spectra are shown in Fig. 5.

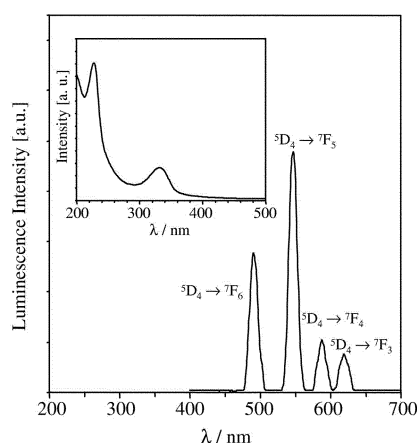


Fig. 5 Luminescence emission spectrum showing $^5\text{D}_4 \rightarrow ^7\text{F}_j$ transitions of Tb^{III} in methanol at 295 K. The inset in this figure is the corresponding excitation spectrum ($\lambda_{\text{em}} = 545 \text{ nm}$).

Luminescence decays of the complexes were investigated by direct excitation of the ligand and by recording the intensity of the emitted light of the $^5\text{D}_4 \rightarrow ^7\text{F}_5$ transition. In all cases, the decay profile fits a single-exponential law, as expected for one discrete $[\text{TbL}_3]$ solution species. In CH_3OH solution at 295 K, these luminescence lifetimes are in the 0.83–0.93 ms range (Table 1). The lifetimes are higher in CH_3OD , which confirms the role played by the vibronic deactivation mechanism involving the O–H oscillators.³⁹ The use of the empirical equation proposed by Horrocks and Sudnick⁴⁰ and the experimental lifetimes in CH_3OH and CH_3OD solutions revealed the average number of methanol molecules (n) in the first coordination sphere of the metal ion to be $n = 2 (\pm 0.5)$ for the four complexes. This is in agreement with the presence of two coordinated solvent molecules and an eight-coordinated structure as we observed in the single-crystal X-ray structure of $[\text{TbI}_3(\text{H}_2\text{O})_2] \cdot \text{H}_2\text{O}$ ¹⁹ and suggests that these four complexes are isostructural. As one can see from Table 1, while the lifetimes are rather similar for these complexes, the quantum yields are very different. The TbI_3 complex is characterized by a quite high quantum

yield (20%). The Tb^{III} complexes of ligands **II**, **III** or **IV** gave less satisfactory results, their quantum yields being more than one or two orders of magnitude lower than that of TbI_3 . As mentioned above, numerous factors influence the overall luminescence quantum yield in photosensitized lanthanide complexes, e.g. the efficiency of $\text{S}_1 \rightarrow \text{T}_1$ energy conversion, the quenching mechanism involving ligand-to- Ln^{III} charge transfer, the energy of the lowest ligand centered triplet state level, the donor–acceptor distance, and the presence of inner-sphere coordinated hydroxylated molecules. In our opinion, the two latter factors do not provide an explanation of the differences in the quantum yield values since the shielding of the metal from solvent molecules in the four systems is similar, the binding functions are equivalent, and the geometrical structures of the complexes are assumed to be analogous. Nor can the experimental results be interpreted by taking into account the involvement of low lying charge-transfer (LMCT) states, which may efficiently deactivate the excited states of the ligand to the ground state. This deactivation pathway, often involved in the case of europium(III) complexes,¹⁶ is not relevant for terbium(III) complexes, as the Tb^{III} ion is very hard to reduce ($E_{\text{red}} = -3.5 \text{ V}$ for the free aqua ion).⁴¹ On the contrary, non-radiative deactivation of the metal emitting state *via* population of the lowest ligand triplet excited state is a quenching mechanism which is commonly observed for Tb^{III} complexes.⁵

Actually, when taking the heavy atom effect into account, complexes of La^{III} , Gd^{III} , Y^{III} or Lu^{III} have been used in various papers to obtain the triplet-state energies.^{14,42–46} These metals have their lowest excited states located at higher energies than the emitting states of aromatic ligands. Therefore, ligand-to-metal energy transfer cannot occur and the consequent metal-centered emission cannot be observed as happens, in contrast, for Tb^{III} and Eu^{III} complexes. However, gadolinium(III) is the most popular metal used in these studies because Gd^{III} and Tb^{III} (Eu^{III}) ions are equal in charge, paramagnetic and very similar in size (eight-coordinated radius: 1.053 Å for Gd^{III} , and 1.040 Å for Tb^{III}).⁴⁷ Consequently, it is widely accepted that these three metal ions induce analogous structures and similar effect on the ligands. So, in order to investigate energy matching between the triplet state of the ligand and the resonance level of Tb^{III} , we recorded the phosphorescence spectra of the free ligands **I–IV** and their Gd^{III} complexes at 77 K in an EtOH–MeOH (4 : 1) glass. Time-resolved luminescence measurements at 77 K showed phosphorescence emission spectra containing one broad band with its maximum ranging from 408 to 550 nm. Fig. 6 reports the results obtained for ligand **IIIH** and the corresponding gadolinium complex. Except for **IIIH**, all the ligands show a red-shift of the LC phosphorescence maximum upon complexation of Gd^{III} , as expected because of the influence of the paramagnetic ion.⁴⁸ Particularly worth noting is the shift of about 90 nm (3450 cm^{-1}) observed for the **III** system. From the

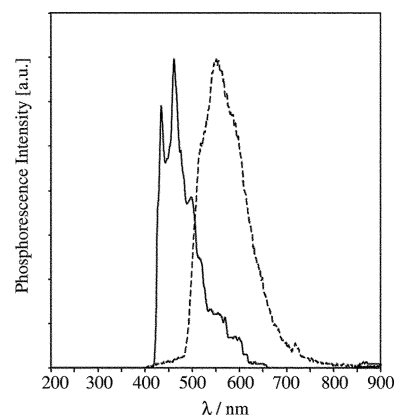


Fig. 6 Normalized time-resolved phosphorescence spectra in an EtOH–MeOH (4 : 1) rigid matrix at 77 K of **IIIH** (plain line) and Gd^{III} complex (dashed line).

Table 2 Phosphorescence properties of ligands **IIH**–**IVH** and their gadolinium complexes. The emission maxima (λ_{\max} in nm) are reported for these structures in an EtOH–MeOH (4 : 1) rigid matrix at 77 K. In parentheses are reported the energy range (in cm^{-1}) corresponding to the left edge of the spectrum and λ_{\max}

L	I	II	III	IV
LH	465 (21500–25000)	463 (21600–26300)	463 ^a (21650–23800)	408 ^b (24500–26650)
LGd	475 (21050–25250)	463 (21600–26300)	550 (18200–20800)	436 (22950–25650)

^a $\tilde{\nu}_{00} = 23000 \text{ cm}^{-1}$. ^b $\tilde{\nu}_{00} = 26000 \text{ cm}^{-1}$.

first peak of the structured phosphorescence profiles of **IIIH** and **IVH**, one can estimate the zero-zero energy of the lowest ligand centered triplet state, which turns out to be 23000 and 26000 cm^{-1} , respectively. Unfortunately, due to the lack of vibrationally structured phosphorescence emission bands, it was not possible to determine the $\tilde{\nu}_{00}$ of the triplet level in **IIH**, **IIIH** and all gadolinium complexes. However, if we inspect the emission domain ranging from the left edge to the maximum of the phosphorescence spectra (*i.e.* an energy range in which lies the zero-zero energy of the lowest LC triplet state), several key points can be stressed. These values (Table 2) show that the triplet state of the complex formed with **III** lies very close or slightly below the $\text{Tb}^{\text{III}} \text{ } ^5\text{D}_4$ emitting state ($E = 20400 \text{ cm}^{-1}$). The extremely poor luminescence of $\text{Tb}^{\text{III}} \text{ } ^5\text{D}_4$ may be, unambiguously attributed to a very efficient back-energy transfer process ($\text{T}_1 \leftarrow \text{Tb}^{\text{III}} \text{ } ^5\text{D}_4$). For the **IV** system, a $\Delta E_{\text{T},\text{M}} (^3E_{00} - E(^5\text{D}_4))$ gap higher than 2500 cm^{-1} may be expected ($2500 \text{ cm}^{-1} < \Delta E_{\text{T},\text{M}} < 5200 \text{ cm}^{-1}$). This energy gap is above the threshold value of 1850 cm^{-1} ,¹² thus the energy back transfer seems to be of minor importance in the $\text{Tb}^{\text{III}} \text{ } ^5\text{D}_4$ complex. Since the $\text{T}_1 \rightarrow \text{Tb}^{\text{III}} \text{ } ^5\text{D}_4$ transfer seems complete, the low quantum yield of $\text{Tb}^{\text{III}} \text{ } ^5\text{D}_4$, by comparison with that of $\text{Tb}^{\text{III}} \text{ } ^5\text{D}_4$, may be probably traced back to a less efficient $\text{S}_1 \rightarrow \text{T}_1$ energy conversion in the former complex. As far as the complexes with ligands **I** and **II** are concerned, no definitive conclusion can be drawn from these experimental data since their $\Delta E_{\text{T},\text{M}}$ gap may lie between 650 and 5900 cm^{-1} .

4 Theoretical results

4.1 Geometries

Comparison with crystallographic data. Firstly, we shall focus on the hydroxamic acid **IIH**. Two tautomeric forms are possible: the hydroxypyridine *N*-oxide and the *N*-hydroxypyridinone (Fig. 7(a)). Ballesteros *et al.* have shown that the second tautomer exists in the crystal phase and in solution,⁴⁹ and have published X-ray data for a compound which corresponds to two *N*-hydroxypyridinone arranged as a cyclic dimer. We have specifically performed DFT-B3LYP calculations on a dimer for the purpose of comparison with experimental data. The results, given in Table 3, show a good agreement between theory and experiments. Following the suggestion of Ballesteros *et al.*, we assume that in solution the *N*-hydroxypyridinone compound exists as a monomer.

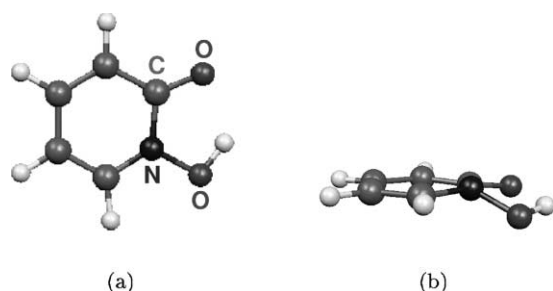


Fig. 7 Optimal geometries of the 1-hydroxypyridin-2-one (**IIH**) in its planar S_0 (a) and T_1 (b) state.

Table 3 Comparison of X-ray data⁴⁹ and theoretical geometry for the (**IIH**)₂ dimer (bond lengths in Å and angles in °)

	IIH X-Ray	B3LYP
H–O _N	1.00	1.018
O _N –N	1.384	1.374
O _C –C	1.252	1.249
C–N	1.380	1.401
N–O _N –H	103	105.2
C–N–O _N	117.7	118.4
N–C–O _C	121.0	121.4
C–N–O _N –H	–70	–67.2

The deprotonated ligand **I** is complexed as a bidentate {O,O} donor with terbium. Beyond the purpose of comparing theoretical and experimental geometries, this case also reveals that, on the theoretical side of this work, LDA calculations predict artefactual geometries. The crystal structure which has been previously reported,¹⁸ does not present any particular symmetry (Fig. 8). However, one can roughly identify a symmetry plane which contains one of the ligands (L_1), the two other ligands (L_2 and L_3) being orthogonal to this plane (see Table 4, $\theta(L_1L_2)$ and $\theta(L_1L_3)$ values).

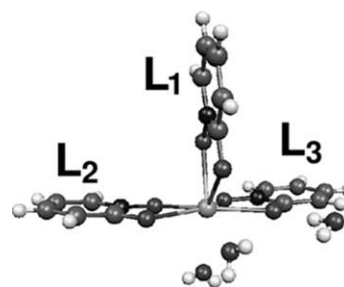


Fig. 8 X-Ray structure for TbI_3 in its ground state S_0 .¹⁸

The terbium ion is surrounded by eight oxygen atoms, two of them belonging to two water molecules in the first coordination sphere. A third water molecule, found in the second coordination sphere of Tb^{III} , is hydrogen-bonded to L_2 . This molecule has not been further considered in the theoretical calculations, since we checked that although its presence does not significantly alter the geometrical parameters, the adiabatic transition energy $\text{T}_1 \rightarrow \text{S}_0$ is very much dependent on it. Indeed, the adiabatic transition energies computed for $\text{TbL}_3(\text{H}_2\text{O})_3$ were not in agreement with the available experimental data, unlike the results obtained for $\text{TbL}_3(\text{H}_2\text{O})_2$, as we shall see in the next section. The geometrical parameters given in Table 4 indicate that there is a good overall agreement between theory and experiment, especially at the B3LYP level of calculation, since the difference between X-ray and theory is in general within the experimental error, *i.e.* 0.04 Å.

The TbI_3 complex was also considered. The removal of the water molecules yields a structure which is almost C_{3v} . While the Tb–O distances may be significantly different with respect to the distances calculated for $\text{TbI}_3(\text{H}_2\text{O})_3$, no significant differ-

Table 4 Comparison of X-ray data and DFT geometry for TbI₃ (bond lengths in Å and angles in °; Tb–X_Y refers to a distance between the Tb atom and the X_Y atom which belongs to ligand L_i). Except for TbI₃, ligands L₂ and L₃ are approximately in the same plane, while ligand L₁ is orthogonal to this plane (see Fig. 8). Labels w₁ and w₂ refer to the two water molecules within the first coordination sphere of the metal ion; θ(L_iL_j) is the angle between two ligands L_i and L_j; a_{OTbO} is the average bite angle of the ligands

	TbI ₃ (H ₂ O) ₂			TbI ₃ B3LYP
	X-Ray ^a	LDA	B3LYP	
Tb–O _{N₁}	2.366	2.291	2.322	2.322
Tb–O _{C₁}	2.370	2.361	2.413	2.340
Tb–O _{N₂}	2.366	2.398	2.411	2.322
Tb–O _{C₂}	2.376	2.334	2.377	2.340
Tb–O _{N₃}	2.411	2.382	2.426	2.322
Tb–O _{C₃}	2.315	2.370	2.428	2.340
O _{N₁} –N ₁	1.353	1.319	1.339	1.339
O _{N₂} –N ₂	1.329	1.319	1.343	1.339
O _{N₃} –N ₃	1.316	1.321	1.342	1.339
O _{C₁} –C ₁	1.268	1.279	1.274	1.276
O _{C₂} –C ₂	1.288	1.283	1.271	1.276
O _{C₃} –C ₃	1.313	1.274	1.275	1.276
C ₁ –N ₁	1.374	1.386	1.392	1.393
C ₂ –N ₂	1.366	1.385	1.393	1.393
C ₃ –N ₃	1.361	1.391	1.392	1.393
Tb–O _{w1}	2.434	2.486	2.610	–
Tb–O _{w2}	2.350	2.431	2.518	–
θ(L ₁ L ₂)	91.9	27.7	86.3	119.9
θ(L ₁ L ₃)	81.9	133.0	89.3	120.1
a _{OTbO}	65.6	66.7	67.1	67.4

^a X-Ray data report the presence of a third water molecule in the second coordination sphere of the terbium ion.¹⁸

ences are observed for the O_N–N, O_C–C and C–N bond lengths. The differences can be justified by the existence of hydrogen bonds observed in our calculations between the hydrogen atoms of the water molecules and the oxygen atoms of the ligands (w₁ with L₁ and L₂ and w₂ with L₂ and L₃). When only distances are considered, LDA performs as well as B3LYP. However, it can be seen in Table 4 that LDA dramatically fails to suitably describe the π interactions between the rings. As a matter of fact, geometry optimization yields an artifactual π-stacking of two ligands, L₁ and L₂, which are not orthogonal, unlike the X-ray and B3LYP structures. This attractive behavior was also observed in the case of the geometry optimization of the complex in its triplet state. Although LDA is usually known to provide accurate geometries, these statements cast suspicion on the ability of LDA to give reasonable geometries and energies for such complexes. From now on, only the B3LYP functional will be used in the framework of DFT calculations. Moreover, since one purpose of this work is to give theoretical insights into the triplet state, we have considered the terbium complex without water molecules in the first and second solvation shells. As a matter of fact, the interactions of water molecules with the ligands by hydrogen bonding make the latter non-equivalent, which may lead to biased conclusions on the nature of the triplet state and the factors influencing the adiabatic T₁ → S₀ transition energy. Besides, it will be shown in the section dealing with adiabatic T₁ → S₀ transitions that the corresponding wavenumbers do not depend on the presence of water molecules in the first coordination shell of the lanthanide ion.

As concerns ligand I[–] complexed with gadolinium, its crystallographic structure consists of [Na₂Gd₂I₈(H₂O)₃]₂·6H₂O units.¹⁹ The sodium counterion links two complex anions *via* the oxygen atoms of I[–] ligands, and it is six-coordinated. Considering the handicap for theory to tackle such large molecules, we have performed geometry optimization at the DFT-B3LYP level of calculation for the GdI₄Na subunit (Fig. 9). The results, reported in Table 5, are in good agreement

Table 5 Comparison of X-ray data¹⁹ and theoretical geometry for the gadolinium complex (bond lengths in Å and angles in °). The values for the four ligands were averaged; θ(L_iL_j) is the angle between two ligands L_i and L_j; a_{OGdO} is the average bite angle of the ligand

	GdI ₄ Na	
	X-Ray	B3LYP
Gd–O _N	2.384	2.437
Gd–O _C	2.383	2.514
O _N –N	1.330	1.332
O _C –C	1.300	1.273
C–N	1.382	1.395
θ(L ₁ L ₂)	105.0	90.1
θ(L ₁ L ₃)	101.6	112.5
θ(L ₄ L ₂)	78.4	103.2
θ(L ₄ L ₃)	85.9	80.4
a _{OGdO}	66.0	63.6

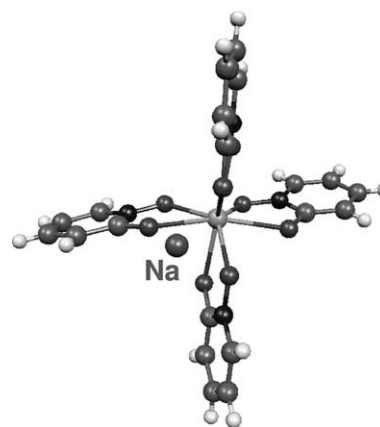


Fig. 9 X-Ray structure for GdI₄Na in its ground state S₀, after ref. 19.

with the experimental data. Two neighbouring ligands are approximately orthogonal. The largest discrepancy is observed for the B3LYP Gd–O_C bond length, too long by 0.126 Å with respect to the experimental value. In so far as the theoretical results obtained for the terbium complex are within the experimental error, a justification for this discrepancy probably lies in the reduction of the [Na₂Gd₂I₈(H₂O)₃]₂·6H₂O unit to the GdI₄Na subunit. In particular, since water molecules interact with the ligands, their absence in the calculation is partly responsible for this disagreement. The origin of this apparent lack of accuracy of theory may also depend on the fact that crystal packing forces shrink bond lengths. However, we assume that there is no prejudicial consequences on the evaluation of the triplet state energy.

Hydroxamic acids LH. The geometries obtained at the DFT-B3LYP level of calculation show that the four hydroxamic acids are planar in their ground state S₀. Selected geometrical parameters and Mulliken atomic charges are given in Table 6. The H–O_N bond length does not depend much on the ligand, the maximum difference, observed between protonated ligands **IH** and **IV'H**, is 0.009 Å. The largest difference between the acids concerns the C–N bond length, which varies from 1.411 to 1.392 Å between molecules **IH** and **IIIH**.

When dealing with the geometries of the ligands in their lowest triplet state T₁, the most striking feature is the pyramidalization of the nitrogen atom in molecules **IH** and **II'H**, while **IIIH** and **IV'H** remain planar. As a matter of fact, for L = **I** (see Fig. 7(b)) and L = **II'**, the O_N and H atoms are no longer in the plane of the ring, the dihedral angle defined by O_N and three atoms of the ring (ω₆) being 23.0 and 27.5° for L = **I** and **II'**, respectively. In the case of ligands **III** and **IV'**, the extent of the conjugated system is more important and may explain that there is no out-of-plane distortion. As can be seen from Table 6, another feature is the rather important lengthen-

Table 6 Geometrical parameters and Mulliken charges of the central ligand in the S_0 and T_1 optimal geometries of LH. The labels of the atoms are defined in Fig. 4; ω_N and ω_O are dihedral angles, defined by atoms $N-C_\alpha-X_\beta-C_\gamma$ and $O_N-C_\alpha-X_\beta-C_\gamma$, respectively ($X=N$ or C according to L)

L	I		II'		III		IV'	
	S_0	T_1	S_0	T_1	S_0	T_1	S_0	T_1
H–O _N	0.997	0.978	0.995	0.979	0.993	1.018	0.988	0.990
H–O _C	1.803	2.043	1.850	2.080	1.832	1.665	1.911	1.882
N–O _N	1.376	1.410	1.371	1.400	1.383	1.340	1.382	1.375
C–O _C	1.243	1.240	1.239	1.238	1.241	1.252	1.235	1.244
N–C	1.411	1.442	1.403	1.454	1.392	1.524	1.395	1.389
ω_N	0.0	2.9	0.0	–0.6	0.0	0.0	0.0	0.0
ω_O	0.0	–23.0	0.0	–27.5	0.0	0.0	0.0	0.0
q_H	0.35	0.34	0.36	0.35	0.35	0.37	0.35	0.36
q_{O_N}	–0.43	–0.42	–0.42	–0.40	–0.43	–0.38	–0.43	–0.41
q_{O_C}	–0.54	–0.44	–0.52	–0.43	–0.53	–0.52	–0.50	–0.50
q_N	–0.16	–0.20	–0.14	–0.17	–0.26	–0.23	–0.17	–0.13
q_C	0.54	0.52	0.52	0.50	0.53	0.51	0.51	0.49

Table 7 Geometrical parameters and Mulliken population analysis in the S_0 and T_1 optimal geometries of TbL_3 ; S_0 : average values for the three ligands; T_1 : the left column corresponds to the excited ligand, the average value for the two non-excited ligands is given in the right column

	I		II'		III		IV'					
	S_0	T_1	S_0	T_1	S_0	T_1	S_0	T_1				
Tb–O _N	2.322	2.445	2.312	2.335	2.385	2.325	2.309	2.418	2.303	2.295	2.411	2.295
Tb–O _C	2.340	2.298	2.321	2.333	2.340	2.320	2.351	2.291	2.333	2.377	2.289	2.362
N–O _N	1.339	1.312	1.340	1.331	1.318	1.331	1.346	1.298	1.346	1.346	1.303	1.346
C–O _C	1.276	1.283	1.279	1.276	1.274	1.278	1.275	1.282	1.277	1.267	1.288	1.269
N–C	1.393	1.499	1.391	1.387	1.491	1.385	1.371	1.498	1.370	1.373	1.488	1.372
a_{OTbO}	67.4	67.8	67.9	67.8	68.0	67.9	67.5	66.7	67.7	67.9	67.8	68.0
ω_N	0.0	2.9	0.0	0.0	2.0	0.0	0.0	0.1	0.0	0.0	0.0	0.0
ω_O	–0.1	31.1	–0.3	–0.3	25.0	0.2	0.3	0.8	0.4	0.4	–0.8	0.5
q_{Tb}	1.40	1.41	1.43	1.44	1.42	1.44	1.43	1.44	1.43	1.44	1.43	1.44
q_{O_N}	–0.59	–0.42	–0.59	–0.58	–0.47	–0.58	–0.61	–0.48	–0.61	–0.60	–0.49	–0.60
q_{O_C}	–0.61	–0.62	–0.62	–0.62	–0.58	–0.62	–0.61	–0.63	–0.61	–0.59	–0.63	–0.60
q_N	–0.05	–0.11	–0.05	–0.02	–0.07	–0.02	–0.14	–0.15	–0.13	–0.07	–0.04	–0.06
q_C	0.56	0.53	0.57	0.56	0.52	0.56	0.56	0.56	0.56	0.55	0.46	0.55

ing of the N–C distance in T_1 with respect to S_0 for L = I, II' and III, which reaches 0.132 Å for IIIH. Another point which must be stressed, although the variations are less important, concerns the H–O_N bond length. It decreases for L = I (0.019 Å) and L = II' (0.016 Å), while it increases for L = III (0.025 Å) and almost remains constant for L = IV' (0.002 Å). As concerns the Mulliken charges, no significant variations in T_1 with respect to S_0 are observed, with the exception of the O_C atom, whose negative charge decreases by approximately 0.1 a.u. for III and II'H.

TbL₃ Complexes. Excited states wavefunctions are often very complex. Various electronic configurations can mix, and the electronic structure of excited states is consequently multi-configurational. In this context, density functional theory can be suspected to yield a poor description of the lowest triplet state. We have thus previously performed CASSCF calculations, in order to check whether the wavefunction of the lowest triplet state is multiconfigurational or can be described by a single configuration. This calculation involves six electrons in seven orbitals. The active space is defined by one π and one π^* orbitals localized on each ligand. The last orbital, selected for allowing the obtaining of a LMCT state, is a d atomic orbital of the metal. The geometry of the TbL₃ complex has been fully optimized without constraints at the CASSCF level of calculation, both for its ground and lowest triplet states. It appears that when the molecule adopts its stable geometry in the lowest triplet state, T_1 can be mainly described by one configuration, which corresponds to a π, π^* excitation strictly localized on one ligand only. According to the density matrix, the occupancy of each of the π and π^* MOs involved in the excitation is close to

1. This ligand does not remain planar, contrary to the two others. As was observed for 1-hydroxypyridin-2-one (IIIH), there is a pyramidalization of the bonds around the nitrogen atom. These results strongly suggest that the excitation is localized on one ligand only. This is also supported by the analysis of the interaction distances between the ion and the ligands. As a matter of fact, while the Tb–O_N and Tb–O_C distances are identical for the three ligands in the ground state of the complex (2.321 and 2.359 Å, respectively) the distance between the excited ligand and the ion significantly changes when the complex is in its T_1 optimal geometry (2.493 Å for Tb–O_N and 2.274 Å for Tb–O_C). It should be noticed that no dramatic change of the interaction distances between the metal and the two other ligands in T_1 with respect to S_0 is observed (2.317 Å for Tb–O_N and 2.340 Å for Tb–O_C). Although these calculations are rather time-consuming, geometry optimizations of the complex in its second triplet state have been performed. The exploration of the T_2 potential energy surface yields a triplet state almost degenerate with T_1 . The optimal geometry corresponds to the distortion of another ligand with respect to T_1 , while the excited ligand in T_1 adopts its S_0 geometry. Again, T_2 is described by a single π, π^* configuration strictly localized on the distorted ligand. Thus DFT, which is formally a single reference method, is expected to be appropriate for describing the lowest triplet state of lanthanide complexes LnL_n. Selected geometrical parameters, obtained in the framework of DFT-B3LYP calculations, which characterize the optimal geometries of TbL₃ complexes in their ground state S_0 and their first triplet state T_1 are given in Table 7, together with Mulliken charges. As concerns TbL₃ in its triplet state T_1 , the main comment is that

Table 8 Geometrical parameters and Mulliken charges in the S_0 and T_1 optimal geometries of GdL_4Na ; S_0 : average values for the four ligands; T_1 : the left column corresponds to the excited ligand, the average value for the three non-excited ligands is given in the right column

	I		II'		III		IV'					
	S_0^a	T_1	S_0^a	T_1	S_0^a	T_1	S_0^a	T_1				
Gd–O _N	2.437	2.629	2.392	2.450	2.571	2.401	2.423	2.506	2.421	2.459	2.521	2.48
Gd–O _C	2.514	2.478	2.512	2.501	2.502	2.503	2.532	2.384	2.537	2.490	2.358	2.50
N–O _N	1.332	1.311	1.329	1.322	1.320	1.319	1.338	1.292	1.339	1.342	1.297	1.343
C–O _C	1.273	1.261	1.278	1.273	1.259	1.278	1.271	1.273	1.274	1.260	1.280	1.261
N–C	1.395	1.503	1.393	1.389	1.482	1.387	1.373	1.496	1.372	1.377	1.494	1.376
a_{OGdO}	63.6	62.5	64.2	64.0	63.4	63.6	63.5	64.2	63.8	64.3	65.5	64.2
ω_N	0.3	1.2	0.1	0.1	2.0	0.1	0.2	1.4	0.2	0.2	0.1	0.1
ω_O	0.7	29.0	0.4	0.5	26.0	0.3	0.2	0.4	0.3	0.4	0.6	0.4
q_{Gd}	1.43	1.47		1.37	1.40		1.37	1.39		1.38	1.40	
q_{O_N}	−0.60	−0.51	−0.58	−0.57	−0.54	−0.55	−0.60	−0.45	−0.61	−0.62	−0.46	−0.63
q_{O_C}	−0.68	−0.58	−0.70	−0.63	−0.50	−0.66	−0.62	−0.59	0.67	−0.58	−0.60	−0.58
q_N	−0.10	−0.11	−0.10	−0.02	−0.05	−0.02	−0.13	−0.15	−0.13	−0.06	−0.04	−0.06
q_C	0.64	0.58	0.64	0.56	0.52	0.56	0.56	0.56	0.57	0.55	0.46	0.55

^a The metal–oxygen distances for the ligand which is considered as excited in T_1 are (in Å): 2.536, 2.542, 2.379, 2.379 for Gd–O_N and 2.461, 2.452, 2.431, 2.441 for Gd–O_C.

it experiences a distortion of one ligand with respect to the optimal geometry in S_0 , and a variation of the distance between that ligand and the Tb^{III} ion, analogous to the CASSCF results. This is also the case for $L = II', III$ and IV' : the geometry of a single ligand significantly changes in T_1 with respect to S_0 . Moreover, as previously found for hydroxamic acids, there is a pyramidalization of the nitrogen atom which results in an out-of-plane motion of O_N for $L = I$ and $L = II'$ ($\omega_O = 31.1$ and 25.0° , respectively), while for $L = III$ and $L = IV'$ the excited ligand remains planar. This ligand, which can be considered as excited in the triplet state, will hereafter be denoted L^* . The variations of Tb–O distances in T_1 with respect to S_0 for the two non-excited ligands do not exceed 0.02 \AA for all the series. This is rather negligible, considering the variations for L^* : the Tb–O_N distance increases by 0.123 , 0.050 , 0.109 and 0.116 \AA for $L = I, II', III$ and IV' , respectively, whereas the Tb–O_C distance decreases by 0.042 , 0.060 and 0.088 \AA for $L = I, III$, and IV' , respectively. Among the series, only the excited ligand II'^* does not exhibit a significant variation of the Tb–O_C distance (0.007 \AA). Considering now all the atoms which form a ring with the terbium ion, the N–O_N, C–O_C and N–C bond lengths do not noticeably vary for the two non-excited ligands. Although the N–O_N and C–O_C bond lengths more significantly change for L^* , the largest variation is observed for the N–C bond length: it increases by more than 0.1 \AA , whatever the ligand. It can also be seen in Table 7 that the bite angle a_{OTbO} remains constant. Considering now the Mulliken charges, the terbium ion is, as expected, positively charged, and its electronic population does not change in the triplet state. The obtained value of 1.4 a.u. can be considered as a large positive charge. Although it is quite far from the formal charge value of $+3$, such values are usually found in such Mulliken analysis on lanthanides. It should be noticed that other charge analysis methods such as NBO yield electronic charges around 2.4 a.u. for lanthanide ions Ln^{III} .⁵⁰ Considering the present Mulliken charge analysis, it is interesting to notice that, similarly to the bond lengths, variations are observed for the excited ligands L^* , and mainly concern the two oxygen atoms.

GdL₄Na Complexes. The geometrical parameters given in Table 8 are presented in a similar way as for TbL₃ complexes. While the three ligands in TbL₃ complexes are equivalent in S_0 , the four ligands of GdL₄Na are not, due to the presence of the sodium counterion. Although the situation seems less clear-cut, similar trends can be drawn: only one ligand can be considered as excited, whereas the three others remain in their ground state. This can be in particular stated from the variation of the Gd–O_N and Gd–O_C bond lengths, as can be seen in Fig. 10. The

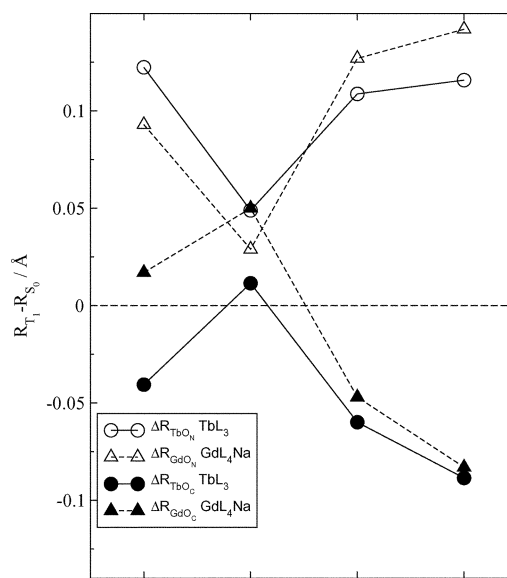


Fig. 10 Variation of the metal–oxygen distances in the T_1 state with respect to the S_0 state for TbL₃ and GdL₄Na. Only the excited ligand L^* is considered.

variations of the metal–oxygen bond lengths in T_1 with respect to S_0 for the whole series of the ligands clearly show a parallelism between the Tb and Gd curves, although they are not exactly superimposable. Similarly to TbL₃, the positive charge on Gd^{III} remains constant in T_1 with respect to S_0 , and the only significant variation concerns the charge of the oxygen atoms. These statements can be summarized by considering the excited terbium and gadolinium complexes as TbL^{*}L₂ and GdL^{*}L₃Na, respectively.

4.2 Adiabatic transition energies

The principal aim of this study is to compare experimental spectroscopic data with theoretical values. It was shown in the previous sections, that geometries obtained at the CASSCF and B3LYP levels of theory compare well, both in the ground state S_0 and in the lowest triplet state T_1 . Thus, the calculations were carried out using the computationally economical methods, *i.e.* restricted and unrestricted B3LYP calculations for S_0 and T_1 , respectively. Since full geometry optimization was achieved, theoretical wavenumbers calculated as $\tilde{\nu}_{\text{adia}}^{\text{theo}} = [E(T_1) - E(S_0)]/hc$ can be compared with the experimental 0–0 transitions ($\tilde{\nu}_{00}^{\text{exp}}$),

Table 9 Theoretical and experimental $T_1 \rightarrow S_0$ transition wavenumbers (in cm^{-1}) of the protonated free ligands LH. An energy range $[\tilde{\nu}_{\text{max}}^{\text{exp}} - \tilde{\nu}_{\text{lw}}^{\text{exp}}]$ (where $\tilde{\nu}_{\text{max}}^{\text{exp}}$ and $\tilde{\nu}_{\text{lw}}^{\text{exp}}$ correspond to the maximum intensity and the left wing of the experimental spectrum, respectively) is given for molecules **IH** and **IIIH** since the vibrational structure is not observable (in emission spectra, $\tilde{\nu}_{\text{lw}}^{\text{exp}} > \tilde{\nu}_{00}^{\text{exp}} \geq \tilde{\nu}_{\text{max}}^{\text{exp}}$)

L	$\tilde{\nu}_{\text{adia}}^{\text{theo}}$	$\tilde{\nu}_{00}^{\text{theo}}$	Exp.
	Theo.	Theo.	
I	23000	21905	21500–25000
II	19813	19001	21600–26300
II'	20300	19411	–
III	21410	20463	23000
IV	24661	23196	26000
IV'	24907	23555	–

although zero-point energy (ZPE) corrections to the theoretical energies should be taken into account for a relevant comparison. Unfortunately, such ZPE corrections could only be systematically computed for the protonated ligands LH, due to the high computational cost for the largest systems.

Hydroxamic acids LH. The theoretical adiabatic transition wavenumbers $\tilde{\nu}_{\text{adia}}^{\text{theo}}$ for acids **IH–IVH** ranged from 19813 to 24907 cm^{-1} (Table 9). ZPE corrections systematically lower the theoretical wavenumbers by approximately 1000 cm^{-1} , which means that the potential energy surface is more flat in T_1 than in S_0 . The substitution of methyl groups with hydrogen atoms only slightly increases the energy of molecules **II'H** and **IV'H** with respect to molecules **IIIH** and **IVH**, and therefore confirms the validity of this simplification. Among all molecules, the lowest triplet state of **IVH** is the less stable with respect to the ground state. All theoretical results are supported by the available experimental work, when available. Similarly, the direct comparison of theoretical and experimental $\tilde{\nu}_{00}$ wavenumbers for molecules **IIIH** and **IVH** indicates that the stability of the triplet state with respect to S_0 is overestimated by approximately $\delta_{00} = 2700 \text{ cm}^{-1}$ for both molecules. To be more precise, the difference $\Delta\tilde{\nu} = \tilde{\nu}_{00}^{\text{exp}} - \tilde{\nu}_{00}^{\text{theo}}$ is 2537 and 2804 cm^{-1} for **IIIH** and **IVH**, respectively. This can be considered as a constant shift of theoretical values with respect to experiments. This is a good result, considering the nature of the ΔSCF method, and in so far as the best *ab initio* methods for the calculation of electronic excited states such as CASPT2 claim an accuracy of $800\text{--}2000 \text{ cm}^{-1}$ on transition energies.³⁰ Considering the adiabatic transition wavenumbers, the difference between theory and experiments is artificially reduced to approximately $\delta = 1700 \text{ cm}^{-1}$. The broadening on the vibrational structure of the experimental emission spectra of **IH** and **IIIH** due to solvent effects does not allow the measurement of $\tilde{\nu}_{00}^{\text{exp}}$ for these two molecules, and accordingly we shall only compare $\tilde{\nu}_{00}^{\text{theo}}$ with an experimental energy range. The theoretical value, augmented or not with δ_{00} , lies within $\tilde{\nu}_{\text{max}}$ and the left wing of the spectrum. Concerning **IIIH**, $\tilde{\nu}_{00}^{\text{theo}}$ corrected by the amount δ yields 21700 cm^{-1} . It is not clear whether in that case the theoretical value is very underestimated or $\tilde{\nu}_{00}^{\text{exp}}$ coincides with $\tilde{\nu}_{\text{max}}^{\text{exp}}$. However, no special reason can be put forward for favouring the former explanation.

Analysis of the theoretical results yields some general trends concerning the link between the extent of conjugation and the position of T_1 with respect to S_0 . As a matter of fact, molecules **IIIH** and **IVH** differ with respect to **II'H** and **IV'H**, respectively, by the substitution of methyl ligands by hydrogen atoms. In other words, the hyperconjugation extends the delocalization of the π electrons of the ring. We have checked that hyperconjugation more stabilizes T_1 than S_0 and thus $\tilde{\nu}_{\text{adia}}^{\text{theo}}(\text{LH}) < \tilde{\nu}_{\text{adia}}^{\text{theo}}(\text{L'H})$. The same conclusion also holds for molecule **IIIH**, which, relative to **IH** is a large conjugated system. As a matter of fact, the $\tilde{\nu}_{00}^{\text{theo}}$ value calculated for **IIIH** is low relative to **IH**. Finally, due to its different chemical structure, the adiabatic

Table 10 Theoretical $T_1 \rightarrow S_0$ transition wavenumbers $\tilde{\nu}_{\text{adia}}$ (in cm^{-1}) of the terbium $\text{TbL}_3(\text{H}_2\text{O})_2$, TbL_3 and gadolinium GdL_4Na complexes. An energy range is given for the experimental emission spectra (see caption of Table 9)

L	Tb (theo.)		Gd	
	$\text{TbL}_3(\text{H}_2\text{O})_2$	TbL_3	Theo.	Exp.
I	22740	23195	22464	21050–25250
II	21616	22790	–	21600–26300
II'	21427	22110	20956	–
III	18634	19096	17853	18200–20800
IV	–	–	–	22950–25650
IV'	22654	22805	22309	–

transition wavenumber of molecule **IVH** cannot directly be compared with the others.

$\text{TbL}_3(\text{H}_2\text{O})_2$, TbL_3 and GdL_4Na complexes. As it was previously recalled, the energy of the lowest triplet state of the ligands complexed with Ln^{III} ions can be probed by phosphorescence experiments on gadolinium complexes, since the lowest electronic level of the gadolinium ion ($^6\text{P}_{7/2}$) lies above 31000 cm^{-1} ,⁵¹ *i.e.* at higher energy than the emitting triplet state of the complexed ligands. Contrarily to experiments, the theoretical determination of the position of the triplet state for terbium complexes is as straightforward as in the case of gadolinium complexes. The triplet state energy of TbL_3 and $\text{TbL}_3(\text{H}_2\text{O})_2$ complexes is almost the same, the triplet state of TbL_3 lying at most 700 cm^{-1} above the triplet level of terbium complexes with water in the first coordination shell (Table 10). This small difference confirms that water molecules present in the first coordination sphere do not play a significant role in the position of the triplet state of the complex, although they have a significant role when considering their ability to quench luminescence *via* vibrational deactivation. As can be noticed according to the results given in Table 10, the replacement of terbium by gadolinium does not affect the triplet state energy level. For instance, T_1 for the $\text{Gd}(\text{II}')_4\text{Na}$ complex lies 471 cm^{-1} below the triplet state of $\text{Tb}(\text{II}')_3(\text{H}_2\text{O})_2$. The theoretical values for $L = \text{I}$ and $L = \text{III}$, augmented with a shift analogous to the δ value introduced for LH hydroxamic acids, are within the experimental energy range. Again, the agreement between theory and experiments confirms the validity of the theoretical method employed in this work.

4.3 Nature of the lowest triplet state

On one hand, α - and β -Kohn–Sham MOs provided by unrestricted DFT calculations do not allow to describe the triplet state T_1 with respect to the ground state S_0 in terms of one or several transitions between MOs. On the other hand, we experienced for the TbI_3 complex that CASSCF calculations performed for the ground state and the first triplet states are very time-consuming, and cannot be handled for exhaustive studies on a wide range of complexes. These CASSCF calculations revealed that the lowest triplet state is described with respect to the ground state by a single excitation between two π MOs localized on the distorted ligand. Since CASSCF calculations are very expensive, we have performed TDDFT calculations in order to get an analysis of T_1 wavefunctions in terms of transitions between MOs. It should be recalled that, although TDDFT deals with the electronic density ρ , the wavefunctions are usually analyzed as linear combinations of single-excited determinants, *i.e.* $\psi = \sum \sum C_{a,b}(\phi_a, \phi_b)$, where ϕ_a and ϕ_b are MOs. We have considered hydroxamic acids LH and terbium complexes TbL_3 ($L = \text{I}, \text{II}', \text{III}, \text{IV}'$) in their T_1 optimal geometry. TD-B3LYP calculations show that in all cases, the wavefunction ψ_{T_1} is mainly described as C_1 (HOMO, LUMO), with $C_1 \geq 0.78$ (see Table 11). The vertical transition energies T_e are also indicated in this table. For LH acids as well as TbL_3

Table 11 Analysis of the TDDFT wavefunction ψ_{T_1} of the lowest triplet state of LH and TbL_3 in the T_1 geometry, optimized at the UB3LYP level of calculation; T_e is the vertical transition energy, in eV (see Fig. 3)

L		I	II'	III	IV'
LH	C_1	0.82	0.86	0.79	0.80
	T_e	2.02	1.67	2.03	2.33
TbL_3	C_1	0.85	0.81	0.84	0.78
	T_e	1.63	1.86	1.57	2.10

complexes, the HOMO and LUMO are π MOs, as can be seen in the case of $L = I$ in Figs. 11 and 12. However the HOMOs and LUMOs involved in the transition are not necessarily the same in LH and TbL_3 compounds. It can be seen on the figures that this is the case for $L = I$, for which the HOMOs are different. However, for both molecules the HOMO has a bonding character between C and N, whereas the LUMO presents an antibonding character. This is consistent with the unrestricted DFT results, which yield larger N–C bond lengths in the T_1 state with respect to the ground state S_0 . Concerning the Tb^{III} complexes, the π MOs which describe the $T_1 \rightarrow S_0$ transition are localized on the ligand which is distorted and for which the interaction distance with the metal significantly changes.

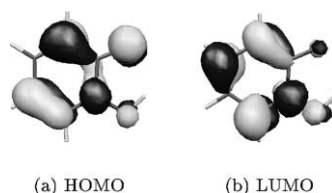


Fig. 11 According to TDDFT calculations the T_1 state of IH is mainly described by the HOMO and LUMO orbitals.

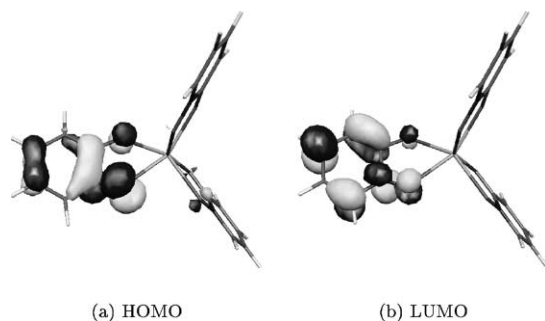


Fig. 12 According to TDDFT calculations the T_1 state of TbI_3 is mainly described by the HOMO and LUMO orbitals.

TDDFT calculations on the three lowest triplet states were done both in the ground state and in the triplet state optimal geometries. The three lowest triplet states are almost degenerate in the S_0 geometry, while T_1 is significantly stabilized in its optimal geometry with respect to T_2 and T_3 which remain degenerate (Table 12). These results suggest that the three triplets are uncoupled.

From a more methodological point of view, it is interesting to compare the adiabatic transition wavenumber calculated in the framework of the Δ SCF method with the value obtained by considering the addition of ΔE obtained at the DFT level and the TDDFT transition energy T_e between S_0 and T_1 (see Fig. 3). This latter quantity, is obtained at different levels of calculation which are formally not consistent, and the $\bar{\nu}_{\text{adia}}$ value computed in this manner (*i.e.* $\Delta E + T_e$) appears to be significantly underestimated for all ligands.

5 Discussion

We shall now propose a rough picture of the energy transfer process which occurs from the triplet states of the ligands

towards the lanthanide ion energy levels. TDDFT calculations show that lanthanide complexes LnL_3 in their ground state have three almost degenerate triplet states. Since triplet states usually have long lifetimes, it can be reasonably assumed that the initial geometry G_{S_0} of the lanthanide complex relaxes in T_1 , leading to a new optimal geometry G_{T_1} (see Fig. 3). We have thus performed CASSCF geometry optimizations in T_1 and T_2 in order to understand the grounds of the phenomena. The calculations clearly show that each triplet state T_i in its optimal geometry G_{T_i} can be considered as typical of a single ligand (L_i) which thus behaves as a chromophore. As a matter of fact, the two singly occupied MOs describing T_1 with respect to S_0 are π orbitals strictly localized on the L_1 ligand (π^{L_1} and π^{*L_1}). The atomic orbitals of the lanthanide which could cast a bridge between two ligands orbitals, are not involved, and no mixing of two π^{L_i} and π^{*L_j} MOs occurs. As a consequence, TbL_3 complexes without solvent molecules are symmetrical in S_0 , exhibiting roughly a three-fold axis, whereas G_{T_1} is unsymmetrical. TDDFT calculations provide an estimation of the energy difference between the symmetrical and unsymmetrical geometries in the lowest triplet state. From the results given in Table 12, we deduce that this energy difference lies within 6500 cm^{-1} (18 kcal mol^{-1}) and 12000 cm^{-1} (34 kcal mol^{-1}) according to the ligand. These results can be related to the work of Amouyal *et al.*, which has experimentally characterized the lowest singlet excited MLCT state of phenylterpyridine– $Ru(II)$ complexes.⁵² This work, also supported by extended Hückel calculations, shows a similarity of the excited-state absorptions to those of the ligand radical anion, and was interpreted as a localization of the excited electron on a single ligand. How can these statements be useful in the framework of experimental works? Consider a lanthanide complex, with three or four identical ligands which are not directly linked together by covalent bonding. Each ligand acts as an individual antenna, which functions in the framework of the whole complex, but which is characterized by a triplet state energy independent of the other antennae. As a consequence, each antenna may provide energy to the lanthanide ion. In so far as the lanthanide complex is surrounded by solvent molecules which dynamically perturb the complex, energy transfer from each of the ligands can alternatively be favored (see also the discussion in ref. 52). The ligands, submitted to a continuous beam of photons, are excited, and the sensitization of the Ln^{III} ion is thus achieved in a very efficient way, the lanthanide complexes considered in this work being multi-chromophoric systems. If we consider now a lanthanide ion surrounded by one antenna only, the energy transfer to Ln^{III} is now ensured by a single collector of photons. Since we propose that the triplet state energy does not significantly change with respect to the multi-chromophoric complex, and considering the energy gap rule, no variation of the luminescence quantum yield should be observed. Our analysis is grounded on the hypothesis (i) that the triplet states are not in equilibrium due to a high energy barrier between them and (ii) that interligand energy transfer does not occur. If that latter point is taken into account, it could mean that the number of antennae may influence the luminescence lifetime. The ligand \rightarrow ligand energy transfer would introduce a delay in the energy transfer towards the emitting level of the lanthanide ion, and consequently the luminescence lifetime should increase. Results recently obtained by Ferrand *et al.*⁵³ are not in contradiction with our conclusions. Finally, it should be noticed that such an “energy reservoir” effect has already been discussed in the case of a bichromophoric system based on a ruthenium–ligand complex linked to an energy reservoir unit.⁵⁴ Our crude models for energy transfer processes in TbL_3 very partially address the more general problem of four-center energy transfer, and the effects of geometry and symmetry on the resonance energy transfer mechanisms, which have been recently studied by means of molecular quantum electrodynamics.⁵⁵ Moreover, we do not know whether the energy transfer is concerted or step-

Table 12 Vertical transition energies T_e of TbL_3 complexes, **L-I**, **II'**, **III**, **IV'** in the S_0 and T_1 geometries obtained at the TDB3LYP level of theory; $\Delta E = E(S_0, G_{T_1}) - E(S_0, G_{S_0})$ (see Fig. 3)

L	I		II'		III		IV'	
	S_0	T_1	S_0	T_1	S_0	T_1	S_0	T_1
T_1	25424	13147	23384	14982	20724	12963	23579	16955
T_2	25440	25414	23386	23502	20733	20601	22583	23425
T_3	25539	25584	23405	23521	20752	20623	22592	23437
ΔE	7589		5384		3952		3599	
$\Delta E + T_e$	20736		20366		16915		20554	
$\tilde{\nu}_{\text{adia}}^{\text{theo}}$	23195		22110		19096		22805	

wise. A corresponding pictorial representation could be streams (the energy provided by the ligands) which feed a river (the energy emitted by the lanthanide ion): do the streams simultaneously or alternately feed the river? We believe that our interpretations and interrogations, undoubtedly controversial and speculative, could participate to the debate between theoreticians and experimentalists.

The results obtained for GdL_4Na complexes do not seem to raise doubts on the previous analysis. Again, one ligand appears excited in the triplet state, the other ones still remaining in their ground state. We have previously shown in Fig. 10 that the variation of the main geometrical parameters which characterize the distortion of the ligand in T_1 with respect to S_0 , that is to say the variation of the metal–oxygen distance, is analogous in TbL_3 and GdL_4Na complexes. However we did not discuss about the factors influencing the triplet state energy. For that purpose, the difference of the Mulliken charges of the oxygen of L^* in T_1 according to the values in S_0 are plotted in Fig. 13. There is a striking parallelism between the curves of Figs. 10 and 13, which strongly suggests that metal–ligand interactions in the triplet state are dominated by the electrostatic interactions between the metal and the surrounding atoms. This is not very surprising, since it is well known that bonding between Ln^{III} ions and anionic ligands in S_0 has mainly a ionic character, even if a charge transfer mechanism may also play a role for weaker ligands.²⁹ It has also been shown that a predominant electrostatic effect is responsible of some geometrical features of lanthanide complexes.⁵⁶ Considering the triplet state, the (π^L, π^{*L}) transition changes the electronic density on the oxygen atoms of L_j , yielding different ligand–metal electrostatic interactions. The triplet state energy thus depends on the nature of the (π^L, π^{*L}) transition, and as a

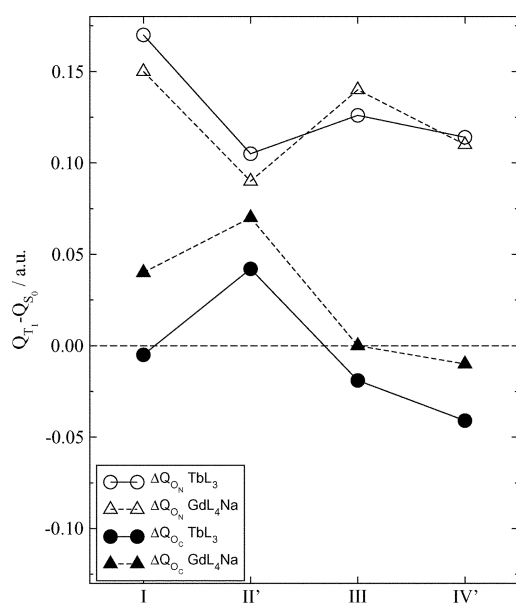


Fig. 13 Variation of the Mulliken charge in the T_1 state with respect to the S_0 state for TbL_3 and GdL_4Na . Only the excited ligand L^* is considered.

consequence it also depends on the variation of electrostatic interactions induced by the variation of the negative charge of the oxygen atoms.

The adiabatic transition energies, compared to data derived from emission spectra, are summarized in Fig. 14. Theoretical results are in general not in disagreement with experimental ones, although the triplet state position is systematically underestimated, in the order of $\delta_{00} = 2700 \text{ cm}^{-1}$. The purpose of the theoretical part of this work being to understand key issues in order to validate a method for designing good luminescent lanthanide complexes in the context of the energy-gap rule, it is very positive that the energy scale provided by the ΔSCF procedure is very similar to the experimental energy scale. Similarly, theory indicates that the triplet state level of molecule **IIIH** lies 2733 cm^{-1} below the triplet state of **IVH**, whereas the difference between the experimental 0–0 transition wavenumbers is 3000 cm^{-1} . The only discrepancy between theory and experiments concerns ligand **II**. As a matter of fact, while the experimental energy range is exactly the same for molecules **IIIH** and GdII_4 , theory finds that the triplet state of the

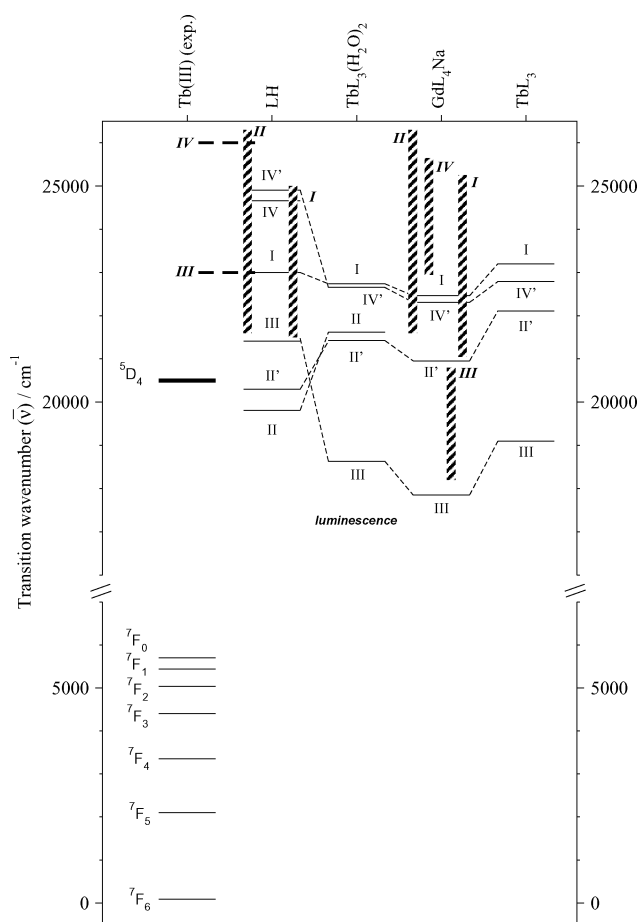


Fig. 14 Comparison of theoretical adiabatic transition wavenumbers $\tilde{\nu}_{\text{adia}}^{\text{theo}}$ (plain lines) and experimental wavenumbers obtained by phosphorescence (dashed lines); ligand labels are indicated in bold italic.

chromophore is destabilized in the complex with respect to the hydroxamate free ligand. No special reason can be put forward for explaining this disagreement.

Concerning ligand **III**⁻ coordinated with gadolinium, it is not possible to strictly assign the $\tilde{\nu}_{00}^{\text{exp}}$ wavenumber, although the phosphorescence emission spectrum presents a vibrational structure at 19300 cm⁻¹. Consequently, the shift between theory and experiments agrees with the energy shift δ , since $\tilde{\nu}_{\text{adia}}^{\text{theo}}$ lies 1450 cm⁻¹ below the estimated value for $\tilde{\nu}_{00}^{\text{exp}}$. It is interesting to note that the effect of complexation is very strong for ligand **III**⁻. As a matter of fact, theoretical as well as experimental results agree for locating the triplet state level of the gadolinium complex stabilized by approximately 3000 cm⁻¹ with respect to the protonated ligand **IIII**. The interpretation does not lie in a different description of the nature of the triplet state of **IIII** and Gd**III**₄Na, since we have checked that, contrarily to ligand **I** (see Figs. 11 and 12), the triplet state of the two molecules correspond to an excitation between the same orbitals. This means that, although the two MOs involved in the excitation do not spread on the metal, the Ln^{III} ion has a strong effect on T₁. Finally, the effect of the complexation is not the same along the series of hydroxamate ligands. Ligand **IV**⁻ also shows a spectacular stabilization of its triplet state due to complexation. In contrast, the lowest triplet state of ligand **II**⁻ is strongly destabilized. As for ligand **I**⁻, its triplet state energy is only slightly lowered.

Coming back to the correlation between triplet state energy and luminescence quantum yield, it is noteworthy that the position of the triplet state, experimentally probed on gadolinium complexes, is implicitly assumed to be the same for other lanthanide complexes. We have shown the transferability of triplet state energy found for gadolinium complexes to terbium complexes. Moreover, we have also performed preliminary calculations on europium complexes which confirm this transferability in the case of ligand **I**⁻. Thus, we have theoretically validated the experimentally implicit hypothesis, on which the energy-gap rule is grounded.

Although the theoretical energy levels for gadolinium complexes reported in Fig. 14 should be shifted for the purpose of quantitative comparison with the experimental energy of the emitting level of the Tb^{III} ion (⁵D₄), it is possible to correlate, in the framework of the energy-gap rule, $\tilde{\nu}_{\text{adia}}^{\text{theo}}$ with the luminescence properties of the terbium complexes. The energy of the T₁ state of ligands **II**⁻ and **III**⁻ is very close to the ⁵D₄ state, thus opening the route to a back-transfer energy process and therefore leading to an inefficient population of the emitting state of the terbium ion. This agrees with the observed luminescence properties, since the two terbium complexes are very weakly luminescent. The quite high luminescence quantum yield of Tb**I**₃ can also be related to the triplet state energy level, which lies approximately 1900 cm⁻¹ above the emitting level of terbium (a value of 3600 cm⁻¹ is more relevant for the purpose of comparison, in so far as the shift between $\tilde{\nu}_{\text{adia}}^{\text{theo}}$ and $\tilde{\nu}_{00}^{\text{exp}}$ is evaluated as 1700 cm⁻¹). Finally, the Tb**IV**₃ complex exhibits a relatively low luminescence quantum yield. The energy-gap rule partially fails for explaining these experimental results. As a matter of fact, the rule cannot explain the different luminescent properties of two terbium complexes whose triplet state energy levels are almost degenerate.

6 Conclusion and outlook

Is it possible to perform theoretical screenings of ligands, prior to chemical synthesis? We have tried to present here some trails, by using quantum chemistry methods, in order to provide good candidates as light collectors, thus attempting to reduce the risk to design good luminescent lanthanide complexes by “*coup de chance*”. We propose, following the suggestion of Mikkala *et al.*,¹² to work in the framework of the energy-gap rule. Although several factors can influence the luminescence properties of

lanthanide complexes, ligands (antennae) should cautiously be designed in order to have a triplet state energy slightly above the emitting level of the lanthanide ion. Although this is not a sufficient condition, it is a necessary condition for obtaining efficient luminescent lanthanide complexes. Recently, in a combined experimental/theoretical work on nine-coordinated lanthanide podates published by the Bünzli group, arguments on the ¹ππ* → ³ππ* ISC have been given by considering the vertical energy gap calculated in the ground state geometry.⁵⁷ As a matter of fact, it is assumed that a large energy gap of 5000 cm⁻¹ is required for an efficient ISC.⁵⁸ While this may possibly provide a first estimation of the ISC efficiency, we believe that an exhaustive theoretical investigation of the spectroscopic properties of these compounds is desirable. However, this would require explorations of excited potential energy surfaces in order to find crossings between surfaces and even conical intersections.^{59–61} Considering the size of these complexes and the difficulty for calculating their electronic structure, this is far beyond the possibilities of *ab initio* theoretical methods. The ΔSCF method, applied in the framework of DFT calculations, has shown its ability to provide reliable results on the lowest triplet state, in agreement with experimental data. It thus seems possible to theoretically provide an energy scale of triplet states of several lanthanide compounds, with a low cost compared to the experimental approach. We also suggest that the number of antennae, while not influencing the triplet state energy, may nevertheless have an influence on the luminescence lifetime: our prescription is to saturate the lanthanide ion with antennae in order to enhance this property. We have also discussed the strong involvement of electrostatic factors in the ligand–metal bonding in the lowest triplet state T₁.

Finally, a more detailed discussion about electrostatic interactions as well as screening of functional groups R in hydroxamate ligands [CO–N(R)O]⁻ will be given in the second paper of this series.

Acknowledgements

F. G., L. M., J.-P. D. and R. P. thank the CALcul en Midi-Pyrénées (CALMIP) and the Centre Informatique National de l'Enseignement Supérieur (CINES) for allocations of computational resources.

References

- 1 P. R. Selvin, *Nat. Struct. Biol.*, 2000, **7**, 730–734.
- 2 H. Hakala, P. Liitti, K. Puukka, J. Peuralahti, K. Loman, J. Karvinen, P. Ollikka, A. Ylikoski, V.-M. Mikkala and J. Hovinen, *Inorg. Chem. Commun.*, 2002, **5**, 1059–1062.
- 3 M. H. V. Werts, R. H. Woudenberg, P. G. Emmerink, R. van Gassel, J. W. Hofstraat and J. W. Verhoeven, *Angew. Chem., Int. Ed.*, 2000, **39**, 4542–4544.
- 4 S. I. Weissman, *J. Chem. Phys.*, 1942, **10**, 214–217.
- 5 N. Sabbatini, M. Guardigli and J.-M. Lehn, *Coord. Chem. Rev.*, 1993, **123**, 201–228.
- 6 P. G. Sammes and G. Yahioglu, *Nat. Prod. Rep.*, 1996, **13**, 1–28.
- 7 L. Maron and O. Eisenstein, *J. Phys. Chem. A*, 2000, **104**, 7140–7143.
- 8 M. Elbanowski and B. Malowska, *J. Photochem. Photobiol., A: Chem.*, 1996, **99**, 85–92.
- 9 H. Bazin, M. Préaudat, E. Trinquet and G. Mathis, *Spectrochim. Acta. Part A*, 2001, **57**, 2197–2211.
- 10 F. R. Gonçalves e Silva, O. L. Malta, C. Reihard, H.-U. Güdel, C. Piguet, J. E. Moser and J.-C. Bünzli, *J. Phys. Chem. A*, 2002, **106**, 1670–1677.
- 11 G. F. de Sá, O. L. Malta, C. de Mello Donegá, A. M. Simas, R. L. Longo, P. A. Santa-Cruz and E. F. da Silva, Jr., *Coord. Chem. Rev.*, 2000, **196**, 165–195.
- 12 M. Latva, H. Takalo, V.-M. Mikkala, C. Matescu, J. C. Rodríguez-Ubis and K. Kankare, *J. Lumin.*, 1997, **75**, 149–169.
- 13 N. Arnaud and J. Georges, *Spectrochim. Acta, Part A*, 2003, **59**, 1829–1840.
- 14 R. D. Archer, H. Chen and L. C. Thomson, *Inorg. Chem.*, 1998, **37**, 2089–2095.

- 15 F. R. Gonçalves e Silva, R. Longo, O. L. Malta, C. Piguet and J.-C. G. Bünzli, *Phys. Chem. Chem. Phys.*, 2000, **2**, 5400–5403.
- 16 R. Longo, F. R. Gonçalves e Silva and O. L. Malta, *Chem. Phys. Lett.*, 2000, **328**, 67–74.
- 17 Z. Barandiarán and L. Seijo, *J. Chem. Phys.*, 2003, **118**, 7439–7456.
- 18 C. Tedeschi, C. Picard, J. Azema, B. Donnadiéu and P. Tisnès, *New J. Chem.*, 2000, **24**, 735–737.
- 19 C. Tedeschi, J. Azéma, H. Gornitzka, P. Tisnès and C. Picard, *Dalton Trans.*, 2003, 1738–1745.
- 20 E. Shaw, *J. Am. Chem. Soc.*, 1949, **71**, 67–70.
- 21 J. Ohkanda, T. Tokumitsu, K. Mitsuhashi and A. Katoh, *Bull. Chem. Soc. Jpn.*, 1993, **66**, 841–847.
- 22 M. Raban, V. A. Martin and L. Craine, *J. Org. Chem.*, 1990, **55**, 4311–4316.
- 23 P. Mamalis, M. J. Rix and A. A. Sarsfield, *J. Chem. Soc.*, 1965, 6278–6288.
- 24 Y. Haas and G. Stein, *J. Phys. Chem.*, 1971, **75**, 3668–3677.
- 25 S. R. Meech and D. Phillips, *J. Photochem.*, 1983, **23**, 193–217.
- 26 M. J. Frisch, G. W. Trucks, H. B. Schlegel, G. E. Scuseria, M. A. Robb, J. R. Cheeseman, V. G. Zakrzewski, J. A. Montgomery, Jr., R. E. Stratmann, J. C. Burant, S. Dapprich, J. M. Millam, A. D. Daniels, K. N. Kudin, M. C. Strain, O. Farkas, J. Tomasi, V. Barone, M. Cossi, R. Cammi, B. Mennucci, C. Pomelli, C. Adamo, S. Clifford, J. Ochterski, G. A. Petersson, P. Y. Ayala, Q. Cui, K. Morokuma, P. Salvador, J. J. Dannenberg, D. K. Malick, A. D. Rabuck, K. Raghavachari, J. B. Foresman, J. Cioslowski, J. V. Ortiz, A. G. Baboul, B. B. Stefanov, G. Liu, A. Liashenko, P. Piskorz, I. Komaromi, R. Gomperts, R. L. Martin, D. J. Fox, T. Keith, M. A. Al-Laham, C. Y. Peng, A. Nanayakkara, M. Challacombe, P. M. W. Gill, B. G. Johnson, W. Chen, M. W. Wong, J. L. Andres, C. Gonzalez, M. Head-Gordon, E. S. Replogle and J. A. Pople, GAUSSIAN 98 (Revision A.11), Gaussian, Inc., Pittsburgh, PA, 2001.
- 27 M. Dolg, H. Stoll, A. Savin and H. Preuss, *Theor. Chim. Acta*, 1989, **75**, 173–194.
- 28 M. Dolg, H. Stoll and H. Preuss, *Theor. Chim. Acta*, 1993, **85**, 441.
- 29 C. Adamo and P. Maldivi, *Chem. Phys. Lett.*, 1997, **268**, 61–68.
- 30 B. O. Roos, *Acc. Chem. Res.*, 1999, **32**, 137–144.
- 31 D. J. Tozer, R. G. Amos, N. C. Handy, B. O. Roos and L. Serrano-Andrés, *Mol. Phys.*, 1999, **97**, 859–868.
- 32 R. Bauernschmitt, R. Ahlrichs, F. H. Hennrich and M. M. Kappes, *J. Am. Chem. Soc.*, 1998, **120**, 5052–5059.
- 33 S. J. A. Ginsbergen, A. Rosa, G. Ricciardi and E. J. Baerends, *J. Chem. Phys.*, 1999, **111**, 2499–2506.
- 34 S. J. A. van Gisbergen, J. A. Groeneveld, A. Rosa, J. G. Snijders and E. J. Baerends, *J. Phys. Chem. A*, 1999, **103**, 6835–6844.
- 35 C. Adamo and V. Barone, *Theor. Chem. Acc.*, 2000, **105**, 169–172.
- 36 G. Schaftenaar and J. H. Noordik, *J. Comput.-Aided Mol. Des.*, 2000, **14**, 123–134.
- 37 S. Portmann and H. P. Lüthi, *Chimia*, 2000, **54**, 766–770.
- 38 F. S. Richardson, *Chem. Rev.*, 1982, **82**, 541–552.
- 39 J. L. Kropp and M. W. Windsor, *J. Chem. Phys.*, 1965, **42**, 1599–1608.
- 40 W. D. Horrocks Jr. and D. R. Sudnick, *Acc. Chem. Res.*, 1981, **14**, 384–392.
- 41 L. R. Morss, *Chem. Rev.*, 1976, **76**, 827–841.
- 42 S. Petoud, J.-C. G. Bünzli, T. Glanzman, C. Piguet, Q. Xiang and R. P. Thummel, *J. Lumin.*, 1999, **82**, 69–79.
- 43 E. Huskowska, I. Turowska-Tyrk, J. Legendziewicz and J. P. Riehl, *New J. Chem.*, 2002, **26**, 1461–1467.
- 44 S. I. Klink, G. A. Hebbink, L. Grave, P. G. B. Oude Alink, F. C. J. M. van Veggel and M. H. V. Werts, *J. Phys. Chem. A*, 2002, **106**, 3681–3689.
- 45 N. Armaroli, G. Accorsi, F. Barigelletti, S. M. Couchman, J. S. Fleming, N. C. Harden, J. C. Jeffery, K. L. V. Mann, J. A. McCleverty, L. H. Rees, S. R. Starling and M. D. Ward, *Inorg. Chem.*, 1999, **38**, 5769–5776.
- 46 G. Zucchi, A.-C. Ferrand, R. Scopelliti and J.-C. G. Bünzli, *Inorg. Chem.*, 2002, **41**, 2459–2465.
- 47 R. D. Shannon, *Acta Crystallogr., Sect. A*, 1976, **32**, 751–767.
- 48 G. E. Buono-Core, H. Li and B. Marciniak, *Coord. Chem. Rev.*, 1990, **99**, 57–87.
- 49 P. Ballesteros, R. M. Claramunt, T. Cañada, C. Foces-Foces, F. H. Cano, J. Elguero and A. Fruchier, *J. Chem. Soc., Perkin Trans. 2*, 1990, 1215–1219.
- 50 L. Perrin, L. Maron and O. Eisenstein, *Faraday Discuss.*, 2003, **124**, 25–39.
- 51 W. T. Carnall, P. R. Fields and K. Rajnak, *J. Chem. Phys.*, 1968, **49**, 4443–4446.
- 52 E. Amouyal, M. Mouallem-Bahout and G. Calzaferri, *J. Phys. Chem.*, 1991, **95**, 7641–7649.
- 53 A.-C. Ferrand, A. Dadabhoy and J.-C. Bünzli, Highly luminescent lanthanide chelate based on the cyclen framework: derivatisation for biological applications. poster, 5th International Conference on f-elements (ICFE5), Geneva, Switzerland, August 2003.
- 54 A. F. Morales, G. Accorsi, N. Armaroli, F. Barigelletti, S. J. A. Pope and M. D. Ward, *Inorg. Chem.*, 2002, **41**, 6711–6719.
- 55 R. D. Jenkins and D. L. Andrews, *J. Chem. Phys.*, 2002, **116**, 6713–6724.
- 56 M. R. Russo, N. Kaltsoyannis and A. Sella, *Chem. Commun.*, 2002, 2458–2459.
- 57 J.-M. Senegas, G. Bernardinelli, D. Imbert, J.-C. Bünzli, P.-Y. Morgantini, J. Weber and C. Piguet, *Inorg. Chem.*, 2003, **42**, 4680–4695.
- 58 F. J. Steemers, W. Verboom, D. N. Reinhoudt, E. B. van der Tol and J. W. Verhoeven, *J. Am. Chem. Soc.*, 1995, **117**, 9408–9414.
- 59 H. E. Zimmerman, *J. Am. Chem. Soc.*, 1966, **88**, 1566–1567.
- 60 M. Klessinger, *Angew. Chem., Int. Ed. Eng.*, 1995, **34**, 549–551.
- 61 M. A. Robb and M. Olivucci, *J. Photochem. Photobiol., A: Chem.*, 2001, **144**, 237–243.